Chapter 6
Space–Time Finite Element Method

In the previous section we discussed some classical methods for the time integration of the differential equations of motion. They have interesting properties, not appreciated by researchers and software developers. In this section we will present the space–time element method. We will give its basic concepts and how to derivate the stepwise equations for this method. We will present the displacement formulation, used in the early stages of the development of the method, and the velocity formulation, which is currently being successfully used for difficult or atypical tasks.

An essential feature which differentiates the space–time element method from traditional approaches to solving initial-boundary problems is its discretization of the differential equation. Classically, two-step interpolation is used, the spatial variables separately from the time. Therefore, in the first stage, the system of partial differential equations is transformed into a system of ordinary differential equations in time of the basic state variables, and further purely numerical procedures are applied for the integration of the differential equations in the time. This approach has its advantages, mainly due to the possibility of selecting the most effective tools separately for each stage, including strict methods. In addition, the passage from the static to the dynamic solution is simpler. Most numerical procedures for static analysis are easy to use in this situation. In fact, the solution of the dynamics reduces to the solution of a set of static tasks (Figure 6.1). The control of the estimation error and the unconditional stability of the solution due to the time step involved in the integration of the differential equation are also significant. All this makes the most popular methods, i.e., the finite element method combined with the method of integration over time, e.g. the Newmark method, a permanent part of the practice of simulation calculations.

One of the drawbacks of the classical approach is the need for partition (discretization) of the considered spatial area which is constant in time (stationary). In this case, the local adaptation of the mesh to the processes involved (e.g., the development of plastic zones, zones of contact, propagation of cracks, the movement of the load) is very difficult. The existing methods of adaptation, including multigrid methods, or moving meshes, are an attempt to adapt a numerical process to a phenomenon, and to remove this defect. However, the first of these techniques is
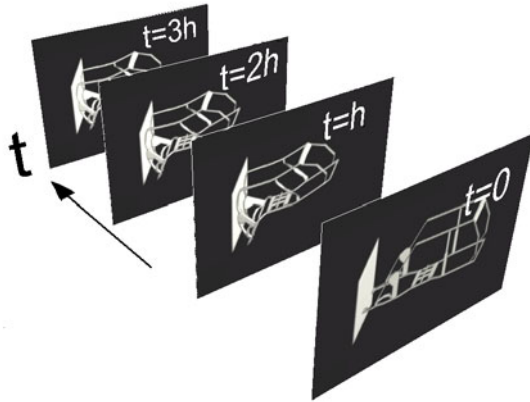
Fig. 6.1 Dynamic problem as a series of static tasks.

generally used for static tasks, while the other, at the present stage of development, can effectively model the task of transport of heat, mass, etc. Certain couplings of the concept of the moving mesh method presented here by space elements should be noted.

The second major drawback is usually the use of the same procedure in time integration for all mesh nodes of the structure. Although it is possible to use locally procedures for the time integration of differential equations with higher accuracy, in order to describe all variables of the physical phenomena within the same time interval (time step), we do not improve the numerical model of the problem. An unconditionally stable scheme of integration of the equations of motion allows of increasing the efficiency of the calculations by lengthening the time step, but at the same time introduces significant amplitude and phase errors, which vary in different zones of the area of the structure. Mesh refining brings, on the one hand, an improvement of the spatial accuracy, but on the other hand can worsen the results of the integration over time. Local interference in the ways of integration in time at the level of a finite element, depending on its size and the characteristics of the material, usually produces difficulties.

Of course all the complexities of the calculations can not categorically determine the advantages and disadvantages of the different groups of methods. Artificial damping of higher frequency vibrations by one method of calculation is a defect in wave problems, but an advantage in the analysis of structural vibrations. The selection of a computational tool is carried out based on the type of task, the phenomena under examination, the required accuracy of the arithmetical operations which can be performed on the computer, and non-substantive factors (e.g., the availability of numerical procedures, one's own experiences, etc.).

The space–time approximation of solutions of dynamic problems lacks some of these drawbacks of the classical numerical methods. However, the method is not
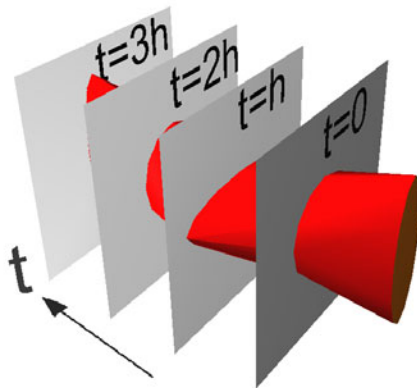
Fig. 6.2 Continuous representation time of a dynamic problem.

perfect. In essence, it reduces to the fact that functions $\mathbf{w}$, characterizing a solution, are described in space–time sub-areas through nodal parameters $\mathbf{q}_e$ (Figure 6.2)

$$\mathbf{w}(\mathbf{x},t) = \mathbf{N}(\mathbf{x},t)\,\mathbf{q}_e. \tag{6.1}$$

The matrix $\mathbf{N}(\mathbf{x},t)$ is a matrix of interpolation functions, depending on the spatial variables and the time[1]. This approach assumes a continuous distribution of characteristic functions, such as displacement or velocity, in the whole space–time domain $\Omega = \{\mathbf{x},t : \mathbf{x} \in V(t), 0 \le t < \infty\}$ where the structure is considered. In discrete time $t_i, i = 0, 1, 2, \ldots$, you can use different bases of nodes (with certain restrictions), and therefore adapt the mesh to current requirements. This has the following possibilities, also shown in Figure 6.3:

- the possibility of redistributing the mesh, depending on the changing distribution of the approximation error,
- moving the zone of a mesh refinement together with a travelling load,
- the ability to adjust the sides of the elements to characteristic lines determined in the space–time domain: the front of the plastic area, the front of the material phase change, in particular—the possibility of modelling a moving edge of a body,
- the use of mesh shapes other than the space-mesh multiplexed meshes: multiplexed networks are the result of an evolution of the spatial grid in the layer of time and the corresponding elements have the same number of nodes in the initial and final time; other meshes, such as simplices, have new, important properties; simplex elements with dimension n have $n+1$ nodes at the initial time and $i+1$ nodes at the final time $(i = 0, 1, \ldots, n)$,

---

[1] For the purpose of comparison, the spatial discretization uses the interpolation formula $\mathbf{u}(\mathbf{x},t) = \mathbf{N}(\mathbf{x})\,\mathbf{q}_e(t)$.
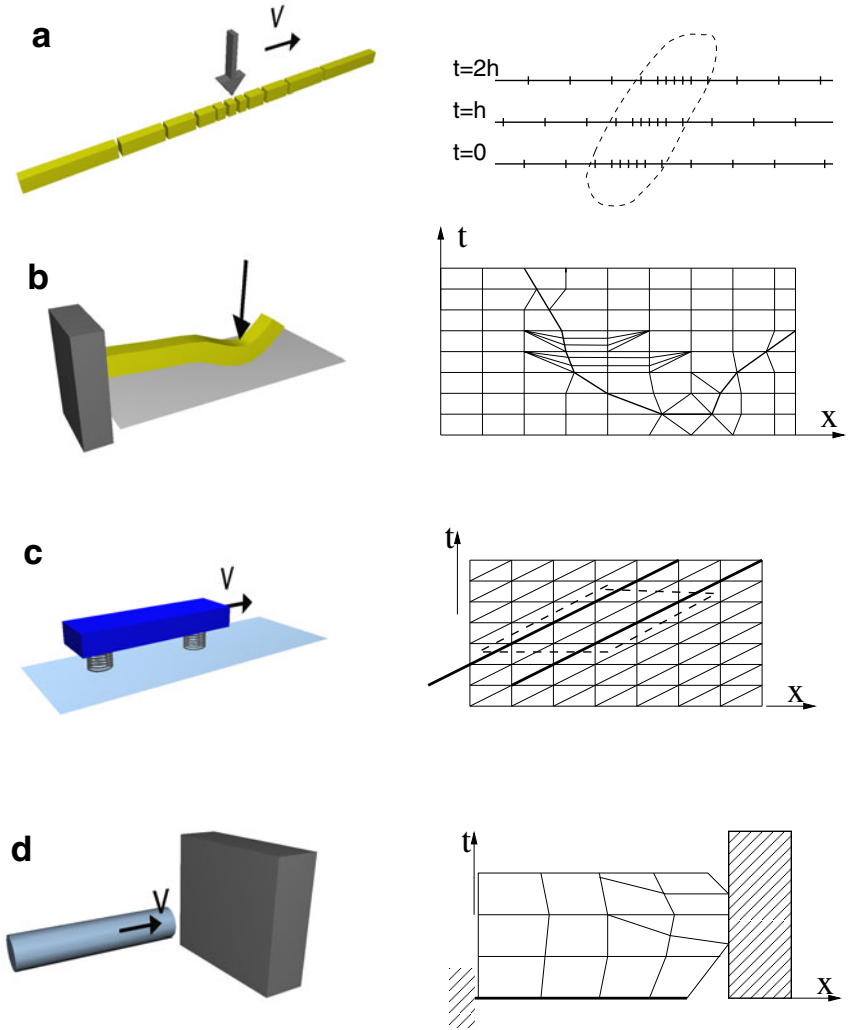
Fig. 6.3 Examples of problems solved in a time-space.

- the possibility of individual formulation of the time integration in an active manner for each spatial element,
- the particular case of space–time approximation can give a classical method of solution, based on fixed grid nodes (evolving only with the material).

This last point can be expanded to a statement that space–time approximation and the resulting space–time element method are a generalization of the finite element method, classically referred to a real space. By real space we mean the space of

spatial variables x, y, z, in contrast to space–time, which is described by the spatial variables x, y, z, and the time t.

The first attempts at space–time modelling of physical problems were published in 1964 by Gurtin [60, 61] and Herrera [63]. Defining a minimized functional, resulting from the theory of convolution, enabled the derivation of relationships between the time variable and spatial variables in space–time domains. These areas can be interpreted as space–time finite elements. Later, in 1969, Oden [105] proposed a generalization of the finite element method. He extended the interpretation of the image of the structure over the time domain. Unfortunately, the interesting idea of a non-stationary partition of a structure into sub-domains proposed in that paper was not continued later on. Fried [55] and Argyris, Scharpf, and Chan [5, 6, 7] began to treat the temporal and spatial variables equally in the formulation of problems. Nevertheless, in the papers of Kuang and Atluri [76] the final digitization in space and time were conducted separately. Dynamic problems were solved with the separation of the temporal and the spatial variables. The physical area of a structure was discretized by one method (finite element method, finite difference method), while the temporal derivatives were integrated with other methods (central difference method, Newmark method, etc.). Numerous papers appeared on the direct integration of the differential equations of motion, assuming a stationary discretization.

Regardless of this direction of research, some elaborations by Kączkowski appeared [77, 79], in which for the first time physical interpretations of certain meanings previously considered in real space were introduced to structural mechanics. This is for example the time-work equation, a mass as a vector, or a space–time stiffness. Simple cases of the vibration of a rod axis and strings were considered.

Another issue raised was the problem of stability [18] and an attempt at synthesis of the space–time formulation [81]. A major contribution was the indication of possibilities for building an unconditionally stable solution by modifying virtual shape functions [73]. Unfortunately, the use of that technology is confined to rectangular space–time elements, whose shape functions can be expressed as a product of terms defining the interpolation functions in space and in time. Further studies were focused on elements other than space–time rectangular shapes. The next important step was to move away from the stationary partition of the spatial structure, and thus to introduce non-rectangular elements in time [17, 18]. This step allowed the application of the method to an entirely new group of issues: contact problems [10] and processes with an adaptation of the mesh [19].

In addition to work on developing the same method, there were many attempts to assess its accuracy and efficiency and to use the space-time element method in various technical issues [12, 13, 14, 114, 136]. In addition to problems of mechanics, issues of heat propagation have been treated [15].

The next step was to incorporate nonlinear effects: geometrical [33, 115, 141] and material nonlinearities [21, 116]. It is also worth mentioning [62], in which the authors use harmonic functions for interpolation in time.

In the paper by Podhorecki [117], rectangular space–time elements known from the paper of Kączkowski (e.g. [79]) were applied to viscoelastic problems. Their considerations were limited to one-dimensional structures. Models of Hooke,

Kelvin–Voigt, Maxwell, and Zener material were used. However, no concrete proposals supported by real examples were given. A group of reviews on the space–time element method are [16, 23].

In this large number of papers, not one has tried to use the opportunities that exist in the method of space–time elements. The considerations were limited to the use of STEM as a method of integration of differential equations. The following sections will demonstrate the equivalence of such procedures using other methods, such as for example the Newmark method. Furthermore, further development of the use of the STEM for modelling dynamic problems is reasonable.

In this chapter, we will present the new opportunities created by changing the spatial approximation continuously in time. In Chapters 6.1 and 6.3, the formulation of the space–time element method will be presented. The resulting equation can be expressed both through displacements and velocities. However, the formulation differs between the two cases. The displacement description leads ultimately to the Galerkin method, applied to space and time, and the velocity description does not lead directly to the Galerkin method. This needs emphasizing. The two formulations have different properties and have different utilities. The derivation of the characteristic matrices of space–time finite elements in the velocity formulation was given. They allow users to easily change the number of nodes in the spatial mesh, and thus to use adaptive techniques. The topological properties of this group of elements allow us to obtain significant computational benefits, thoroughly discussed in the next chapter.

Another, separate, characteristic group of space–time elements are the elements with simplicial shape. The properties of derived with their use in the solutions will be discussed in Chapters 6.7 and 6.8. The most important feature here is to obtain the final triangular matrix of the system of algebraic equations. This results in some interesting applications, such as the possibility of limiting the speed of propagation of information in a discrete system. This allows us in some cases to restrict an infinite domain to a small number of finite elements. An example of this approach is presented in [11].

The space–time formulation was used to model contact zones variable in time [20, 34]. Dynamic contact conditions were written, which were applied to lightweight engineering tasks. A dense digitization of time was used. This allowed an accurate determination of the contact forces. A way of eliminating discontinuities of the velocity function at the ends of the time domain of a contact was presented. The experience gained was used to model the rail–wheel contact area and the generation of corrugations. With material nonlinearities, iterative solutions of a nonlinear equation of motion were linked with the integration of this equation in time. Relevant numerical schemes were presented.

Examples of calculations of both test and real engineering problems confirm the effectiveness of the techniques described. However, many issues will certainly arise. This is not the final state of the development of the space–time description of the dynamics of structure.

In numerical examples, as the primary system of units we use the SI system. In order to improve the conditioning the of resulting matrices of algebraic equations

in computer calculations, the respective multipliers were scaled by multipliers: the length by 10^{-2}, the mass by 10^{-3}, and time by 10^{-6}. This allowed us to avoid severe range differences in solid material properties and thus get rid of certain numerical difficulties. Due to the fact that many numerical examples are only illustrative, we used non-dimensional values. In the comparative examples and more complex tasks, complete, actual values of all parameters are given.

6.1 Formulation of the Method—Displacement Approach

Although the first mention of the possibility of nonstationary discretization of a structure appeared in the paper of Oden[105], the truly systematic introduction of the space–time element method was by Kączkowski [77, 78]. He introduced terms which look unusual in engineering. A material point appearing in the discussion at time t_0 and at place x_0, moves to the position x_1 at time t_1. In the system of coordinates (x,t), these two positions of the material point designate the section. To describe the motion of the mass as part of the oscillator, at both ends of the so called vector imaging the life of the mass, we define some physical quantities such as momentum or force from an elastic element, and between the two ends we take into account the impact of external effects. Writing the corresponding equation of virtual work, we can make the state at t_1 depend on the state at t_0. This way we get the stepping scheme of calculating the differential equation of motion.

Described in a series of new papers, one look at the dynamics detects a fault—it was conceptually complicated. The dynamics was not seen as a process of binding phenomenon in both space and time. While spatial discretization could be performed relatively easily, even in complex problems, time was treated with great care. During the rapid development of the process automation of the calculation, when the resulting classic finite element models took into account increasingly complex physical phenomena, it was difficult to produce adequate interest in a new and difficult technique.

The failure by the scientific world to model difficult tasks of structural dynamics and wave phenomena in the full sense of the time-space, and the underdevelopment of efficient algorithms in some types of problems, had for many years left undone tasks such as the description of continuous problems involving a point mass moving over an assumed trajectory or alterations in the local rigidity.

Further on we will derive the basic equations of the displacement version of the space–time finite element method as presented in papers published slightly later. We will show the typical course of treatment of an axially vibrating rod. We will obtain sample solutions and show the simplicity of the numerical calculations. Anticipating the content, we will show the identity of some solutions with the solutions obtained using the finite difference method applied to the spatial derivatives when the central difference method is applied to the velocity and acceleration. We will describe the finite space–time elements of some selected types of structures. Taking these descriptions as a point of departure one could, repeating these procedures, determine the characteristic matrices according to one's own needs.

We will consider a continuous solid, closed in the domain $\overline{V}$, and being a sub-area of the Euclidean space E^3. V denotes the interior of the area, and ∂V its boundary, which, in turn, is the sum of ∂V_t and ∂V_u, where, respectively, the displacement and stress boundary conditions will be imposed. We will consider the motion of the body during the interval $[0,T]$. The variables included in the description, such as the displacement vector $\mathbf{u}$, the velocity $\mathbf{v}$, the vector of mass forces $\rho\mathbf{f}$, the symmetric tensor of the stress field σ, and the deformation field ε, are defined on the Cartesian product set $V \times [0,T]$. The vector of surface forces $\widehat{\mathbf{t}}$ is defined on the product $\partial V \times [0,T]$. We assume that all functions are sufficiently continuous. Geometrically and physically linear problems are described by the following system of equations:

- geometric equations

$$\varepsilon(\mathbf{x},t) = \frac{1}{2}\left(\operatorname{grad}\mathbf{w} + \operatorname{grad}^T\mathbf{w}\right), \quad (\mathbf{x},t) \in V \times [0,T], \tag{6.2}$$

- physical equations

$$\sigma(\mathbf{x},t) = \mathbf{E}\varepsilon, \quad (\mathbf{x},t) \in V \times [0,T], \tag{6.3}$$

- equations of dynamical equilibrium

$$\operatorname{div}\sigma^T + \rho\mathbf{f} = \rho\frac{\partial\mathbf{v}}{\partial t}, \quad (\mathbf{x},t) \in V \times [0,T], \tag{6.4}$$

- boundary conditions

$$\sigma\,\mathbf{n} = \widehat{\mathbf{t}}(\mathbf{x},t), \quad (\mathbf{x},t) \in \partial V_t \times [0,T], \tag{6.5}$$

$$\mathbf{w}(\mathbf{x},t) = \widehat{\mathbf{u}}(\mathbf{x},t), \quad (\mathbf{x},t) \in \partial V_u \times [0,T], \tag{6.6}$$

- initial conditions

$$\mathbf{w}(\mathbf{x},t) = \mathbf{w}^0, \quad (\mathbf{x},t) \in \overline{V} \times \{0\}, \tag{6.7}$$

$$\dot{\mathbf{w}}(\mathbf{x},t) = \mathbf{v}^0, \quad (\mathbf{x},t) \in \overline{V} \times \{0\}. \tag{6.8}$$

In the above relationship, $\mathbf{w}^0$ and $\mathbf{v}^0$ define the initial displacement and the velocity, respectively, and $\widehat{\mathbf{w}}^0$, the displacements on the boundary ∂V_u. This system is a local formulation. The existence and uniqueness of the solution can be proved as in [104]. A global formulation can be achieved by multiplying (6.4) by the variation of the virtual function of displacements $\delta\mathbf{w}(\mathbf{x},t)$

$$\delta\mathbf{w}(\mathbf{x},t) = \begin{cases} 0, & (\mathbf{x},t) \in \partial V_u \times [0,T] , \\ \text{any}, & (\mathbf{x},t) \in (\overline{V} - \partial V_u) \times [0,T] . \end{cases} \tag{6.9}$$

After integration we obtain

$$\int_{t_0}^{t_1}\int_V \left(\operatorname{div}\sigma^T + \rho\mathbf{f} - \rho\dot{\mathbf{v}}\right)\delta\mathbf{w}\,dV\,dt + \int_{t_0}^{t_1}\int_{\partial V_t}\widehat{\mathbf{t}}\,\delta\mathbf{w}\,d(\partial V)\,dt = 0. \tag{6.10}$$

Integrating by parts, we obtain

$$\int_{t_0}^{t_1} \int_V \rho \left(\mathbf{f}\delta\mathbf{w} + \dot{\mathbf{w}}\,\delta\dot{\mathbf{w}} \right) dV\, dt + \int_{t_0}^{t_1} \int_{\partial V_t} \widehat{\mathbf{t}}\,\delta\mathbf{w}\,d(\partial V)\, dt = \int_{t_0}^{t_1} \int_V \sigma\delta\varepsilon\, dV\, dt. \quad (6.11)$$

The area in which (6.11) is described should now be discretized. The area $\{\overline{V}, 0 \leq t \leq T\}$ is divided into subareas, which are in fact space–time finite elements. The simplest possible divisions are shown in Figure 6.4a. The space–time layers $[t_i \leq t \leq t_{i+1}]$, $i = 0, 1, \ldots, n-1$, are cut in a semi infinite band, where n is the number of layers in the interval [0, T], and inside them there are isolated elements of the geometry, fixed in time. A more complex partitioning of the space–time layer is also possible (Figure 6.4b). We will return to this issue in later chapters.

The simplest element is separated from the time-space by planes $t = t_i$ and $t = t_{i+1}$. They are hyper-prisms (hyper-prisms are prisms in space of dimension higher than 3), which are finite elements, stretched in time (Figure 6.5). The values of the unknowns, in our case the displacements $\mathbf{w}$ and their derivatives ($\dot{\mathbf{w}}$, ε, σ), real and
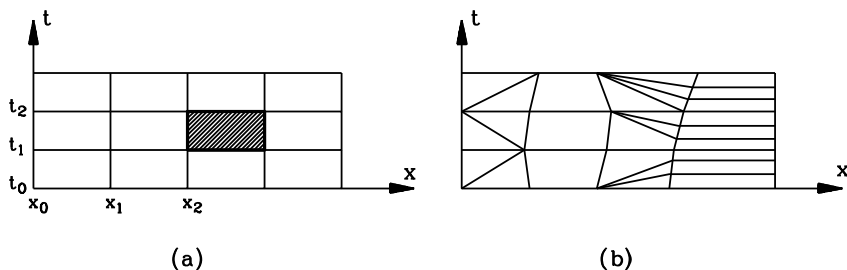

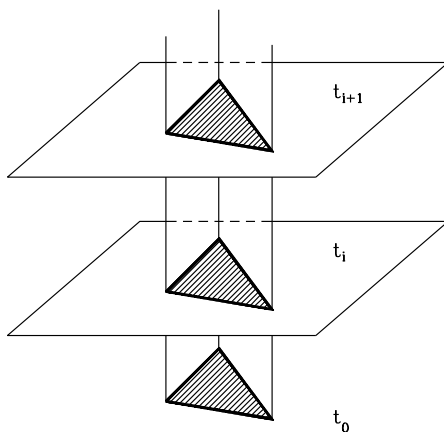**Fig. 6.4** Examples of space–time element mesh: (a) stationary, (b) nonstationary.

Fig. 6.5 Space–time element, separated from the time-space.

virtual, in the area of the space–time element are interpolates on the basis of the values of the nodal displacements $\mathbf{q}$:

$$
\begin{aligned}
\mathbf{w}(\mathbf{x},t) &= \mathbf{N}(\mathbf{x},t)\,\mathbf{q}\,, & \delta\mathbf{w}(\mathbf{x},t) &= \mathbf{N}^*(\mathbf{x},t)\,\delta\mathbf{q}\,, \\
\dot{\mathbf{w}}(\mathbf{x},t) &= \dot{\mathbf{N}}(\mathbf{x},t)\,\mathbf{q}\,, & \delta\dot{\mathbf{w}}(\mathbf{x},t) &= \dot{\mathbf{N}}^*(\mathbf{x},t)\,\delta\mathbf{q}\,, \\
\varepsilon(\mathbf{x},t) &= \mathbf{B}(\mathbf{x},t)\,\mathbf{q}\,, & \delta\varepsilon(\mathbf{x},t) &= \mathbf{B}^*(\mathbf{x},t)\,\delta\mathbf{q}\,, \\
\sigma(\mathbf{x},t) &= \mathbf{E}\mathbf{B}(\mathbf{x},t)\,\mathbf{q}\,.
\end{aligned}
\tag{6.12}
$$

These relationships apply separately to each element of time-space. Quantities marked by $(.)^*$ refer to a virtual state. The matrix $\mathbf{B}$ can easily be created by letting a suitable differential operator $\mathscr{D}$ act on the matrix of shape functions $\mathbf{N}$: $\mathbf{B} = \mathscr{D}\mathbf{N}$, where $\mathscr{D} = \frac{1}{2}\left(\mathrm{grad} + \mathrm{grad}^T\right)$. It should be emphasized that the vector $\mathbf{q}$ consists of the displacements in the space–time element nodes. These nodes have different time coordinates.

Linear (affine) shape functions $\mathbf{N}(\mathbf{x},t)$ express the boundary conditions on the free end $\partial\mathbf{w}/\partial\mathbf{n} = 0$ in a natural way. In the case of the element of length b, with time step Δt, they are satisfied approximately. Refining the digitization ($b \to 0$) in the extreme element $\partial\mathbf{w}/\partial\mathbf{n} \to 0$ ($\partial\mathbf{w}/\partial\mathbf{n} \sim 1/N$, where N is the number of nodes in the mesh).

Taking into account (6.12) in (6.11) gives a quadratic form, expressing the equality of the work of the internal and external forces in the interval $[t_0, t_1]$:

$$
\sum_{e=1}^{NE}\left((\Pi_e^T\delta\mathbf{q}_e)^T\Pi_e^T\mathbf{K}_e^*\Pi_e\cdot\Pi_e^T\mathbf{q}_e - (\Pi_e^T\delta\mathbf{q}_e)^T\Pi_e^T\mathbf{Q}_e\right) = 0.
\tag{6.13}
$$

Here, NE is the number of space–time elements in the structure. The matrices Π_e are zero–one matrices assigning the places of the elemental matrices and vectors to places in the global matrix and vector of the structure. Their form depends on the topology of the mesh discretization. The number of rows equals the number of unknowns associated with a single element, and the number of columns equals the number of unknowns in the structure. These matrices define an aggregation of the matrix elements.

The matrix $\mathbf{K}_e^*$ is the space–time stiffness element matrix

$$
\mathbf{K}_e^* = \mathbf{K}_e + \mathbf{M}_e.
\tag{6.14}
$$

We give here the form of the stiffness matrix $\mathbf{K}_e$ and the inertia matrix $\mathbf{M}_e$ of the element

$$
\mathbf{K}_e = \int_{t_0}^{t_1}\int_V (\mathscr{D}\mathbf{N})^T\,\mathbf{E}\,\mathscr{D}\mathbf{N}\,\mathrm{d}V\,\mathrm{d}t,
\tag{6.15}
$$

$$
\mathbf{M}_e = -\int_{t_0}^{t_1}\int_V \left(\frac{\partial N}{\partial t}\right)^T \mathbf{R}\,\frac{\partial N}{\partial t}\,\mathrm{d}V\,\mathrm{d}t,
\tag{6.16}
$$

where $\mathbf{E}$ is a matrix of elasticity, $\mathscr{D}$ is a matrix of differential operators, and $\mathbf{R}$ is the unitary matrix of inertia.

If we assume a viscoelastic body described by the Kelvin–Voigt model, where the relationship between the stress and the strain is written

$$\sigma = \left(\mathbf{E} + \eta_w \frac{\partial}{\partial t} \right) \varepsilon \tag{6.17}$$

(η_w—viscous damping coefficient) and if into the equation (6.10) we introduce a dissipative term, depending on the speed of displacement [17], then (6.14) takes the form

$$\mathbf{K}_e^* = \mathbf{K}_e + \mathbf{M}_e + \mathbf{W}_e + \mathbf{Z}_e, \tag{6.18}$$

where $\mathbf{W}_e$ and $\mathbf{Z}_e$ are the terms of internal damping and external damping, respectively:

$$\mathbf{W}_e = \int_{t_0}^{t_1} \int_V (\mathscr{D}\mathbf{N})^T \eta_w \frac{\partial}{\partial t} \mathscr{D}\mathbf{N} \, dV \, dt, \tag{6.19}$$

$$\mathbf{Z}_e = \int_{t_0}^{t_1} \int_V \mathbf{N}^T \eta_z \frac{\partial}{\partial t} \mathbf{N} \, dV \, dt. \tag{6.20}$$

$\mathbf{Q}_e$ is the vector of the external load acting on the space–time element e:

$$\mathbf{Q}_e = \int_{t_0}^{t_1} \int_V \mathbf{N}_e(\mathbf{x},t) \widehat{\mathbf{t}}(\mathbf{x},t) \, dV \, dt. \tag{6.21}$$

It can be obtained from (6.5). Since (6.13) must be satisfied with any variation of displacements and for the entire space–time area, we can write

$$\sum_{e=1}^{E} \left(\Pi_e^T \mathbf{K_e} \Pi_e \cdot \Pi_e^T \mathbf{q}_e - \Pi_e^T \mathbf{Q}_e \right) = \mathbf{0}. \tag{6.22}$$

The above system of algebraic equations includes the entire space–time domain $[0,T]$. The solution is obtained using the initial conditions (6.7) and (6.8). The displacement condition (6.7) can easily be discretized:

$$\mathbf{q}_0 = \sum_{e=1}^{E} \Pi_e^T \int_{V_e} \mathbf{N}_e(\mathbf{x},0) \, \mathbf{w}(\mathbf{x},0) \, dV_e. \tag{6.23}$$

In turn, the velocity condition (6.8 requires the use of an additional difference formula to express velocities at the initial moment by means of two displacement vectors $\mathbf{q}_0$ given by the expression (6.23) and $\mathbf{q}_{-1}$ (when $t = -h$), for example, as follows:

$$\mathbf{q}_{-1} = \mathbf{q}_0 - \dot{\mathbf{q}}_0 h, \quad \dot{\mathbf{q}}_0 = \sum_{e=1}^{E} \Pi_e^T \int_{V_e} \mathbf{N}_e(\mathbf{x},0) \, \dot{\mathbf{w}}(\mathbf{x},0) \, dV_e. \tag{6.24}$$

Consider now one time layer, $t_i \leq t \leq t_{i+1}$. Divide the unknown displacements by the displacements with respect to time t_i and the displacements with respect to time t_{i+1}. Then the coefficients matrix of equation (6.22)) can be divided into four submatrices, separating a submatrix $\mathbf{A}_i$ with rows and columns relating to the time t_i,

the submatrix $\mathbf{B}_i$ with rows relating to time t_i and columns relating to time t_{i+1} and similarly $\mathbf{C}_i$ and $\mathbf{D}_i$, but with rows relating to time t_{i+1}. We can therefore write

$$\begin{bmatrix} \mathbf{A}_i \ \mathbf{B}_i \\ \mathbf{C}_i \ \mathbf{D}_i \end{bmatrix} \left\{ \begin{matrix} \mathbf{q}_i \\ \mathbf{q}_{i+1} \end{matrix} \right\} = \left\{ \begin{matrix} \mathbf{Q}_i \\ \mathbf{Q}_{i+1} \end{matrix} \right\}. \tag{6.25}$$

Now the process of summation in (6.22) refers to the addition of the matrix (6.25). A tridiagonal block matrix of a system of equations is formed, with size corresponding to the number of moments into which the space–time region was partitioned. The following is the block form corresponding to (6.22)

$$\begin{bmatrix} \mathbf{A}_1 \ \mathbf{B}_1 \\ \mathbf{C}_1 \ \mathbf{D}_1 + \mathbf{A}_2 \ \ \mathbf{B}_2 \\ \quad \mathbf{C}_2 \ \ \mathbf{D}_2 + \mathbf{A}_3 \ \ \mathbf{B}_3 \\ \quad \cdots \ \cdots \ \cdots \\ \mathbf{0} \qquad \mathbf{C}_{i-1} \ \mathbf{D}_{i-1} + \mathbf{A}_i \ \mathbf{B}_i \\ \qquad\qquad \cdots \ \ \cdots\cdots \end{bmatrix} \left\{ \begin{matrix} \mathbf{q}_1 \\ \mathbf{q}_2 \\ \mathbf{q}_3 \\ \vdots \\ \mathbf{q}_{i-1} \\ \mathbf{q}_i \\ \mathbf{q}_{i+1} \\ \vdots \end{matrix} \right\} = \left\{ \begin{matrix} \mathbf{Q}_1 \\ \mathbf{Q}_2 \\ \mathbf{Q}_3 \\ \vdots \\ \mathbf{Q}_{i-1} \\ \mathbf{Q}_i \\ \mathbf{Q}_{i+1} \\ \vdots \end{matrix} \right\}. \tag{6.26}$$

The system (6.26) can be solved in stages, with one line of this system for each step. So we have to solve

$$\mathbf{C}_{i-1}\,\mathbf{q}_{i-1} + (\mathbf{D}_{i-1} + \mathbf{A}_i)\,\mathbf{q}_i + \mathbf{B}_i\,\mathbf{q}_{i+1} = \mathbf{Q}_i, \quad i = 1, 2, \dots \,. \tag{6.27}$$

We can now return to the conditions (6.23) and (6.24) and to the solutions of the system (6.26) in the first steps. At $\mathbf{q}_0 \neq \mathbf{0}$ and $\dot{\mathbf{q}}_0 \neq \mathbf{0}$ we have:

$$\mathbf{C}_{-1}\mathbf{q}_{-1} + (\mathbf{D}_{-1} + \mathbf{A}_0)\,\mathbf{q}_0 + \mathbf{B}_0\,\mathbf{q}_1 = \mathbf{Q}_0, \quad \mathbf{C}_{-1} = \mathbf{C}_0, \quad \mathbf{D}_{-1} = \mathbf{D}_0. \tag{6.28}$$

The simplest case occurs when $\mathbf{q}_0 = \mathbf{0}$ and $\dot{\mathbf{q}}_0 = \mathbf{0}$. Then we have:

$$\mathbf{B}_1\,\mathbf{q}_2 = \mathbf{0}. \tag{6.29}$$

The only unknown displacement vector in (6.27) is $\mathbf{q}_{i+1}$. The vectors $\mathbf{q}_{i-1}$ and $\mathbf{q}_i$ were obtained in the previous steps, i.e., $i-2$ and $i-1$. An efficient construction of the system of equations and its solution can be carried out following the scheme below, using the auxiliary vector $\mathbf{r}$:

$$\mathbf{r} = \mathbf{C}_{i-1}\,\mathbf{q}_{i-1} + \mathbf{D}_{i-1}\,\mathbf{q}_i \,, \tag{6.30}$$
$$\mathbf{A}_i\mathbf{q}_i + \mathbf{B}_i\,\mathbf{q}_{i+1} = \mathbf{Q}_i - \mathbf{r} \,.$$

Here we must mention [72], in which the author gives a way of constructing the so-called space–time macroelement. It consists of eliminating every second (or, more generally, every 2^n) layer of nodes, by removing every second row in the system (6.26). In this way, the time step increases to $2^n\,h$. This technique requires the

inversion of a submatrix and is effective only in the case of constant matrices $\mathbf{A}_i$, ..., $\mathbf{D}_i$. par The stability of numerical schemes with a stationary mesh, based on the displacements, is described in [73, 88]. Depending on the selection of the virtual shape functions we can obtain unconditionally or conditionally stable variants of the method. These considerations can be summarized by saying that the formulations in the papers cited above are equivalent to Newmark methods, and have all their properties, including those concerning stability.

6.1.1 Space–Time Finite Elements in the Displacement Description

6.1.1.1 Bar Element

We will deal with the derivation of the fundamental equations of the equilibrium of forces in the space–time element method with a stationary spatial mesh. This issue will be treated for the example of the simplest equation describing the axial vibration of a bar. The differential equation of an axially vibrating bar is identical to the equation of a vibrating string

$$\rho A \frac{\partial^2 w(x,t)}{\partial t^2} = EA \frac{\partial^2 w(x,t)}{\partial x^2} + p(x,t) . \tag{6.31}$$

Here, E is the elastic modulus, A—the cross sectional area, ρ—mass density, and p—external load. Multiplying this equation by a virtual displacement function $w^*(x,t)$ and integrating over the present area $x \in [0,b]$ and $0 \le t \le h$ we get the equation of virtual work

$$\int_0^h \int_0^b w^*(x,t)\rho A \frac{\partial^2 w(x,t)}{\partial t^2} \mathrm{d}x\mathrm{d}t = \int_0^h \int_0^b w^*(x,t)EA \frac{\partial^2 w(x,t)}{\partial x^2} \mathrm{d}x\mathrm{d}t +$$
$$+ \int_0^h \int_0^b w^*(x,t)p(x,t)\mathrm{d}x\mathrm{d}t . \tag{6.32}$$

We lower the degree of the derivative by integrating the first term by parts with respect to t and the second term with respect to x. We recall that w^* has equals zero at the points $x = 0$ and $x = b$ and also $t = 0$ and $t = h$. We do not need to do so, if at a later stage we can provide a non-zero second derivative of the solutions, and in practice a sufficiently high degree polynomial for approximation of the solutions. Then we can write

$$\int_0^h \int_0^b \frac{\partial w^*(x,t)}{\partial x} EA \frac{\partial w(x,t)}{\partial x} \mathrm{d}x\mathrm{d}t - \int_0^h \int_0^b \frac{\partial w^*(x,t)}{\partial t} \rho A \frac{\partial w(x,t)}{\partial t} \mathrm{d}x\mathrm{d}t =$$
$$= \int_0^h \int_0^b w^*(x,t)p(x,t)\mathrm{d}x\mathrm{d}t . \tag{6.33}$$

Now we suggest a way of interpolating the values of $w(x,t)$ and its virtual equivalent, $w^*(x,t)$, based on the nodal values of $\mathbf{q}_e$ in the element. Take a linear interpolation in the form

$$w(x,t) = [N_1(x,t), N_2(x,t), N_3(x,t), N_4(x,t)] \begin{Bmatrix} q_1 \\ \vdots \\ q_4 \end{Bmatrix} = \mathbf{N}\mathbf{q}_e . \qquad (6.34)$$

The real shape functions can be written in local coordinates (ξ, τ). Then $N_i = 1/4\,(1+\xi\,\xi_i)(1+\tau\,\tau_i)$, where ξ_i, τ_i are the coordinates of the vertices of the rectangle $\{\xi, \tau : -1 \leq \xi \leq 1, -1 \leq \tau \leq 1\}$. The transition between a local and global coordinate system is defined by $x = \sum_{i=1}^{4} N_i\, x_i$ and $t = \sum_{i=1}^{4} N_i\, t_i$. Then we assume virtual shape functions in the same way. After the substitution of w and w^* into (6.33), we get the total energy of the system, comprising terms describing the internal energy, the kinetic energy, and the work of the external forces on the virtual displacements. The energy minimization condition reduces to zero the derivatives with respect to all unknowns q_i, $i = 1, \ldots, 4$. In the end, we obtain a system of four equations

$$\left(\frac{EAh}{6b} \begin{bmatrix} 2 & -2 & 1 & -1 \\ -2 & 2 & -1 & 1 \\ 1 & -1 & 2 & -2 \\ -1 & 1 & -2 & 2 \end{bmatrix} - \frac{\rho ab}{6h} \begin{bmatrix} 2 & 1 & -2 & -1 \\ 1 & 2 & -1 & 2 \\ -2 & -1 & 2 & 1 \\ -1 & -2 & 1 & 2 \end{bmatrix} \right) \begin{Bmatrix} q_1 \\ q_2 \\ q_3 \\ q_4 \end{Bmatrix} =$$

$$= \begin{Bmatrix} F_1 \\ F_2 \\ F_3 \\ F_4 \end{Bmatrix} . \qquad (6.35)$$

The first matrix is the stiffness matrix, with coefficients

$$K_{ij} = \frac{EAh}{12b}\xi_i\xi_j(3 + \tau_i\tau_j) , \qquad (6.36)$$

and the second matrix is the inertia matrix, with coefficients

$$M_{ij} = -\frac{\rho Ab}{12h}\tau_i\tau_j(3 + \xi_i\xi_j) . \qquad (6.37)$$

By introducing the notation $k = c^2 h^2/b^2$ and $c^2 = E/\rho$, we can write the symmetric space–time stiffness matrix $\mathbf{K}_e$ contained in the equation (6.35) in parentheses

$$\mathbf{K}_e = \frac{\rho ab}{6h} \begin{bmatrix} 2k-2 & -2k-1 & k+2 & -k+1 \\ & 2k-2 & -k+1 & k+2 \\ & & 2k-2 & -2k-1 \\ & & & 2k-2 \end{bmatrix} . \qquad (6.38)$$

6.1.1.2   Beam Element

Consider a rectangular beam element of medium thickness. Nodes may be in the general case shifted in space within time interval. One case is when the element is a rectangle in space.

Assume a linear displacement

$$\left\{ \begin{array}{c} w \\ \theta \end{array} \right\} = \left\{ \begin{array}{c} a_1xt + a_2x + a_3t + a_4 \\ b_1xt + b_2x + b_3t + b_4 \end{array} \right\} = \left\{ \begin{array}{c} \mathbf{ag} \\ \mathbf{bg} \end{array} \right\} , \tag{6.39}$$

where $\mathbf{g}(x,t) = [xt, x, t, 1]$ is a vector of monomials. If we denote by $\mathbf{G}$ the matrix composed of the vectors $\mathbf{g}(x_i, t_i)$ defined at element nodes, then we can extract from the inverse matrix $\mathbf{G}^{-1}$ the columns marked by $\mathbf{r}_i$:

$$\mathbf{G}^{-1} = \begin{bmatrix} \mathbf{g}(x_1,t_1) \\ \mathbf{g}(x_2,t_2) \\ \mathbf{g}(x_3,t_3) \\ \mathbf{g}(x_4,t_4) \end{bmatrix}^{-1} = \begin{bmatrix} x_1t_1 & x_1 & t_1 & 1 \\ x_2t_2 & x_2 & t_2 & 1 \\ x_3t_3 & x_3 & t_3 & 1 \\ x_4t_4 & x_4 & t_4 & 1 \end{bmatrix}^{-1} = [\mathbf{r}_1, \mathbf{r}_2, \mathbf{r}_3, \mathbf{r}_4] . \tag{6.40}$$

We obtain the shape functions $\mathbf{N}$ as

$$\mathbf{N} = [\mathbf{N}_1, \mathbf{N}_2, \mathbf{N}_3, \mathbf{N}_4] , \quad \mathbf{N}_i = \mathbf{gr}_i \begin{bmatrix} 1 & 0 \\ 0 & 1 \end{bmatrix} . \tag{6.41}$$

The differential operator $\mathscr{D}$ describes deformations depending on displacements

$$\mathscr{D} = \begin{bmatrix} \frac{\partial}{\partial x} & 1 \\ 0 & \frac{\partial}{\partial x} \end{bmatrix} , \quad \varepsilon = \mathscr{D}\mathbf{N}\mathbf{q} . \tag{6.42}$$

The corresponding matrix of elasticity, in turn, is

$$\mathbf{E} = \begin{bmatrix} \frac{GA}{K} & 0 \\ 0 & EI \end{bmatrix} . \tag{6.43}$$

In the particular case where the space–time element is a rectangle, the shape functions are simpler:

$$\mathbf{N} = \left[\left(1 - \frac{x}{b}\right)\left(1 - \frac{t}{h}\right), \frac{x}{b}\left(1 - \frac{t}{h}\right), \left(1 - \frac{x}{b}\right)\frac{t}{h}, \frac{x}{b}\frac{t}{h} \right] . \tag{6.44}$$

The stiffness matrix $\mathbf{K}$ and the inertia matrix $\mathbf{M}$ are determined as integrals over the element Ω (see (6.15), (6.16), (6.19), and (6.20))

$$\mathbf{K} = \int_{\Omega} (\mathscr{D}\mathbf{N})^T \mathbf{E}\mathscr{D}\mathbf{N} d\Omega , \tag{6.45}$$

$$\mathbf{M} = \int_{\Omega} \left(\frac{\partial}{\partial t}\mathbf{N} \right)^T \mathbf{E} \frac{\partial}{\partial t}\mathbf{N} d\Omega . \tag{6.46}$$

6.2   Properties of the Integration Schemes

The classic methods of the analysis of the vibrations of structures usually use one and the same method of integration for the whole structure and all its degrees of freedom. Often, some sub-areas, or some kinds of degrees of freedom do not require a high accuracy in the calculations and a small step-size for the integration. An example might be the axial movement of frames of tall buildings. From the engineering point of view, it is important to analyse the flexural motion of the rod components. In this direction, the stiffness of the structural elements is much lower than the axial stiffness. The axial vibrations of bars have minimal amplitudes and less practical importance. Therefore, we can analyse them with less accuracy. The same occurs for structures placed on the ground, for the interaction between the structure and the ground or with a surrounding fluid. The inertia and stiffness of the two subdomains differ significantly. A short time step in the explicit procedures, chosen accouding to the criterion of stability or accuracy, greatly lengthens the calculations. A reasonable procedure would be to use explicit methods for modelling the ground and implicit methods for modelling the structure. The application of mixed operators to integration opens new opportunities for improving the accuracy efficiency of the solving of complex tasks. A description of the issues concerning both the statics and dynamics are presented, for example, in [109]. Techniques based on the algebraic partition of the operator are called operator splitting techniques and based on the structure partition – domain splitting.

Operator splitting methods and semi-implicit methods can be classified as being part of the same group of methods. A characteristic feature here is a willingness to preserve the unconditional stability of the integration, or a desire to achieve a significant lengthening of the critical step of integration. Such an increase in the integration step can be achieved by, for example, macro-elements, where in the description of consecutive time layers, intermediate algebraic degrees of freedom are eliminated. In this way, the time span of the integration step increases. The same technique applies to spatial variables.

6.2.0.3   Information Flow

Calculation methods may differ in another important feature: the information flow diagram in a mesh in space and time. Consider, for example, the system of algebraic equations arising (at every step of the calculation) from the method of central differences with a diagonal inertia matrix. An external impulse acting as a load on the last degree of freedom in the mesh produces a non-zero displacement of this degree of freedom (Figure 6.6). In the next step, the product of the matrix $2\mathbf{M} - h^2\mathbf{K}$ with the vector of displacements $\mathbf{q}_i$ results in a vector with nonzero last two entries. This in turn gives the nonzero last two entries of the solution vector $\mathbf{q}_{i+1}$. In this way, in each successive step in the calculation, the influence of the initial single pulse of the external force $\mathbf{F}_0$ propagates to the neighbouring nodes in the finite element mesh at a rate of one node in one step. The speed of the information flow is thus the average of $\Delta x/\Delta t$, where Δx is the spatial distance between neighbouring nodes.
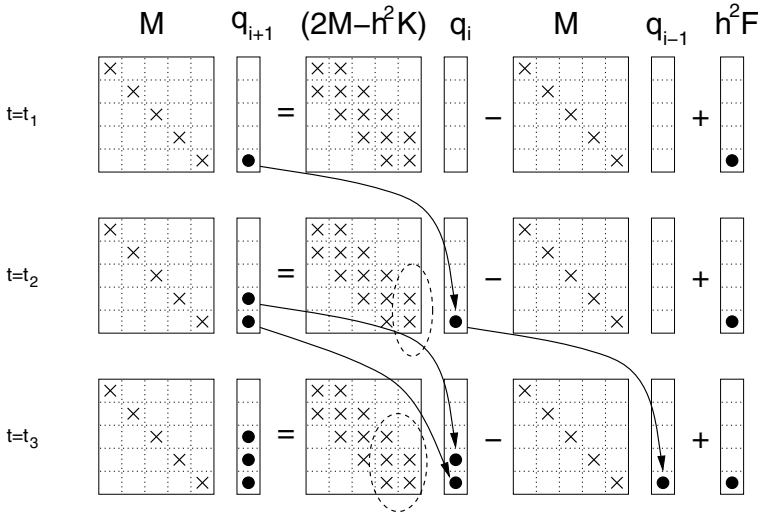
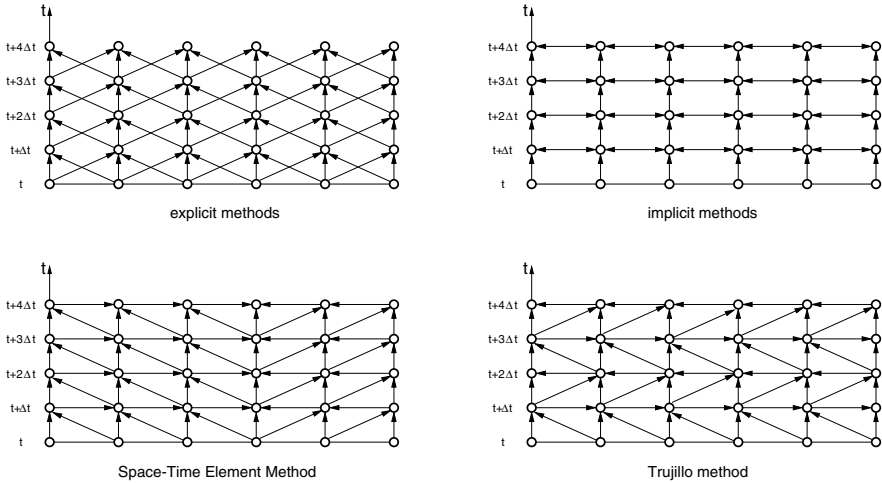**Fig. 6.6** Mechanism for information flow between successive steps in the central difference method.

Fig. 6.7 Flow of information in various calculation methods.

In the case of implicit methods we deal with the solution of algebraic equations with a full matrix of coefficients. A single external impulse transfers immediately to all unknowns of the system. In turn, as will be discussed in subsequent chapters, the space–time finite element method with simplicially shaped elements has a reduced speed of information flow to the sloping sides of the space–time mesh. The Trujillo method has a limited speed of information flow among the grid nodes. A schematic of the flow of information in selected calculation methods is given in Figure 6.7.

6.2.1 Accuracy of Methods

In Table 6.1, the global error of the selected computational methods is estimated. In
principle, all methods have a global error of the second order. The estimates included
in Chapters 6.3.4 and 6.4.1, especially Equation (6.103), are relevant here.

Table 6.1 Global error of the calculation methods.

method	error degree	coefficient
Runge–Kutta 2nd order	h^2	1/6
central difference m.	h^2	1/6
space–time elem. m.	h^2	1/12
space–time elem. m. higher order formulae (6.103)	h^3	1/12
Newmark m. $\beta=1/4$	h^2	$(\sqrt{2}-1)/2$
Runge–Kutta 4th order	h^4	1/120

6.3 Velocity Formulation of the Method

The method in terms of displacements has many features similar to those of the cen-
tral difference method. The schematic calculation is based on displacements in three
consecutive moments of time. Depending on the features of the virtual displacement
functions adopted, the method in its displacement variant may be conditionally or
unconditionally stable. The solution scheme for the equation of motion can be ob-
tained using velocities as the basic quantities for description of the system. This
solution method does not differ from obtaining the solution in terms of displace-
ments. We create a virtual work equation, which takes its minimum value subject
to the given velocities at the beginning and end of the time interval. In this way, we
associate known quantities at the earlier time with those at the later time.

In the following sections, we will present a procedure in the case of a single
degree of freedom. Then we will repeat it for the case of a string. We will use
a variety of shapes for the velocity virtual functions. We will compare the schemes
obtained from the Newmark time integration method with those from other methods
of calculation.

6.3.1 One Degree of Freedom System

Let us elaborate a solution scheme for the vibrations of a material point described
by

$$m\frac{\mathrm{d}v}{\mathrm{d}t} + kx = 0 .$$

(6.47)

We assume a linear distribution of the real velocity v in the time interval h $(0 \leq t \leq h)$

$$v = \left(1 - \frac{t}{h}\right)v_0 + \frac{t}{h}v_1 \ . \tag{6.48}$$

The displacement $x(t)$ is described by the integral

$$x(t) = \int_0^t v\,\mathrm{d}t = x_0 + \frac{h}{2}\left[1 - \left(1 - \frac{t}{h}\right)^2\right]v_0 + \frac{t^2}{2h}v_1 \ . \tag{6.49}$$

Displacement $x(t)$ is linearly dependent on the speed v_0 and v_1 set at the ends of the interval $[0,h]$. Now we take the form of the virtual function. We can choose it among many possible functions. The selected function at the ends of the time interval must have value equal to zero. Below we take a virtual velocity function as Dirac distribution, depending on parameters α $(0 \leq \alpha \leq 1)$ and speed v_1:

$$v^* = v_1 \cdot \delta\left(\frac{t}{h} - \alpha\right) \ . \tag{6.50}$$

If we multiply the differential equation of motion (6.47), which in fact is the equation of equilibrium of forces acting on a material point, by the virtual velocity (6.50), we get the equation of virtual power. After integration it in time interval $[0,h]$ we obtain the equation of virtual work

$$\int_0^h v^* \frac{1}{h}(v_1 - v_0)\,\mathrm{d}t + \int_0^h v^* \frac{k}{m}x(t)\,\mathrm{d}t = 0 \ . \tag{6.51}$$

Finally we get the equation which allows us to determine the speed at the next while, based on the velocity and displacement at the previous while

$$v_1 = \frac{1 - \frac{kh^2}{2m}[1 - (1-\alpha)^2]}{1 + \frac{k\alpha^2 h^2}{2m}}v_0 - \frac{k}{m}\frac{h}{\left(1 + \frac{k\alpha^2 h^2}{2m}\right)}x_0 \ . \tag{6.52}$$

The same can be written symbolically

$$v_1 = T\,v_0 + B x_0 \ . \tag{6.53}$$

It remains to determine from the velocity v_0 and v_1 the missing displacement x_1. We use the relationship

$$x_1 = x_0 + h[(1-\beta)v_0 + \beta v_1] \ . \tag{6.54}$$

A little further on we shall show that the stable solution is obtained in a certain range of parameter α at $\beta = 1 - \alpha$. Taking it into account we can write the final formula

$$x_1 = x_0 + h[\alpha v_0 + (1-\alpha)v_1] \ . \tag{6.55}$$

In the particular case $\alpha = 1/2$ the equation (6.55) is identical to the equation (6.49) adopted at $t = h$, i.e., $x_1 = x_0 + h(v_0 + v_1)/2$.

Introducing the notation $\kappa = h^2 k/m$ we can describe the transition to the next moment as follows:

$$\left\{ \begin{matrix} v_1 \\ x_1 \end{matrix} \right\} = \begin{bmatrix} 1 - \dfrac{2\alpha\kappa}{2+\alpha^2\kappa} & -\dfrac{2\kappa}{h(\alpha^2\kappa+2)} \\[2ex] 3h - \dfrac{2h(\alpha\kappa+2)}{\alpha^2\kappa+2} & \dfrac{2\kappa(\alpha-1)}{\alpha^2\kappa+2}+1 \end{bmatrix} \left\{ \begin{matrix} v_0 \\ x_0 \end{matrix} \right\}. \tag{6.56}$$

The transition matrix $\mathbf{T}$ is a 2×2 matrix. We can use it to determine the stability criterion for any value of the time step, and so as $h \to \infty$. Let us determine the eigenvalues of this matrix:

$$\lim_{h\to\infty} \lambda_{1/2} = \frac{\alpha^2 - 1}{\alpha^2} \pm \frac{i\sqrt{2\alpha^2 - 1}}{\alpha^2}, \tag{6.57}$$

and their moduli:

$$\lim_{h\to\infty} |\lambda_{1/2}| = \begin{cases} 1, & \text{if } \sqrt{2}/2 \le \alpha \le 1, \\[1ex] \dfrac{1}{\alpha^2}\sqrt{\alpha^4 - 4\alpha^2 + 2}, & \text{if } 0 \le \alpha < \sqrt{2}/2. \end{cases} \tag{6.58}$$

Both eigenvalues have modulus unity when $\alpha \ge \sqrt{2}/2$. In this range of the parameter α, we obtain an unconditionally stable solution scheme. This important feature allows us to safely carry out the calculations for systems with a large number of degrees of freedom, or for systems with evolving material properties and geometry. In such cases, the unconditional stability of the method is necessary.

The ability to damp higher frequency vibrations while leaving the basic frequencies undamped is also important. Many authors have devoted papers to this problem (for example [64, 67]). If we modify the formula (6.54) so that the speed will be determined at a slightly later time than $\alpha - 1$, we get this damping effect. The parameter β should be modified to

$$\beta = 1 - \frac{\alpha}{1+\gamma}, \quad 0 \le \gamma \le 1. \tag{6.59}$$

Figure 6.8 shows the value of the spectral radius in its dependence on γ with increasing values of relative the time step h/T. They are made with $\alpha = 0.8$ and $\alpha = 0.9$. The bold lines are the levels plotted for each increment of 0.02. With $\gamma = 0.0$, the spectral radius ρ is unity, by the previous considerations. The next Figure 6.9 shows the logarithmic damping decrement at $\alpha = 0.8$ and 0.9, depending on the size of the relative time step h/T. The levels of both figures are plotted for each increment of 0.05.

Sample calculations of the vibrations of a single point, with the initial conditions $x_0 = 0$ and $v_0 = 1$ and at $\alpha = 0.5$ are shown in Figure 6.10, and at $\alpha = 1.0$ in Figure 6.11.
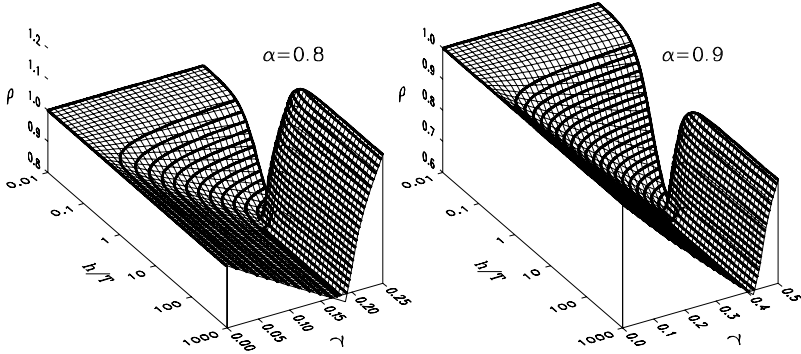
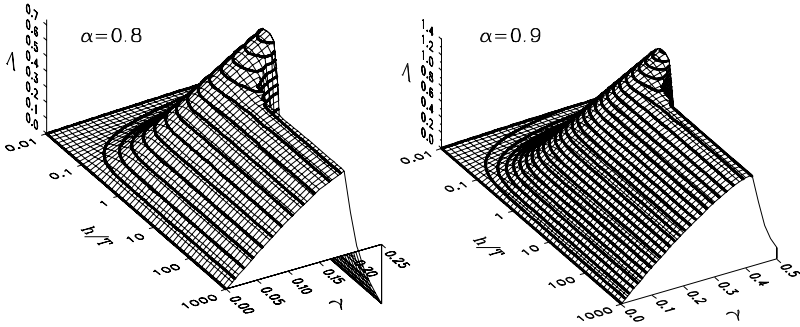**Fig. 6.8** Spectral radius ρ depending on the parameter γ for $\alpha = 0.8$ and $\alpha = 0.9$.

Fig. 6.9 Logarithmic damping decrement Λ depending on the parameter γ at $\alpha = 0.8$ and $\alpha = 0.9$.
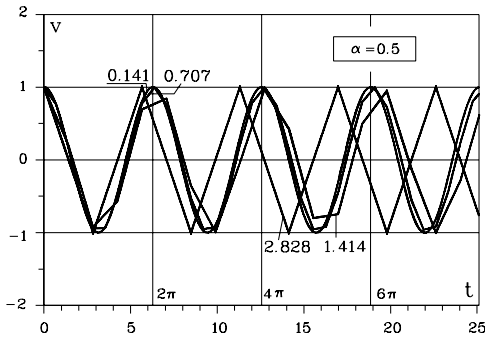

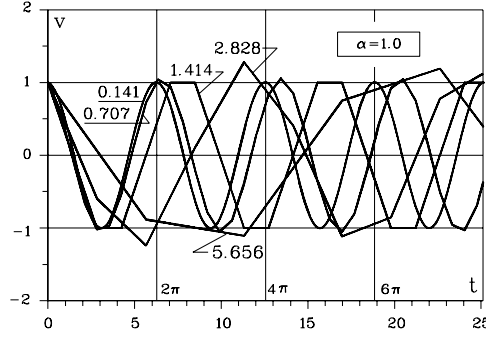**Fig. 6.10** Velocity v determined with various time step, at $\alpha = 0.5$.

Fig. 6.11 Velocity v determined with various time step, at $\alpha = 1.0$.

6.3.2 Discretization of the Differential Equation of String Vibrations

The differential equation of string vibration is as follows:

$$N\frac{\partial^2 w}{\partial x^2} - \rho A\frac{\partial^2 w}{\partial t^2} - \eta\frac{\partial w}{\partial t} - q(x,t) = 0 \ . \tag{6.60}$$

Here, N is the string tension, A is the cross sectional area, ρ is the mass density, η is the damping coefficient, and q is the external load. The wave speed in the string at $\eta = 0$ is $c = \sqrt{N/\rho}$.

Consider the equation in the region $\Omega = \{(x,t): 0 \leq x \leq b, \ 0 \leq t \leq h\}$. The virtual power equation is created by multiplying (6.60) by the virtual speed $v^*(x,t)$

$$\int_0^b v^*(x,t)\left(\frac{\partial^2 w}{\partial x^2} - \frac{1}{c^2}\frac{\partial^2 w}{\partial t^2} - \eta\frac{\partial w}{\partial t} + \tilde{q}(x,t)\right)dx = 0 \ . \tag{6.61}$$

$\tilde{q}$ denotes the load scaled by N: $\tilde{q} = q/N$. The total virtual work in the area Ω is

$$\int_0^h\int_0^b v^*(x,t)\left(\frac{\partial^2 w}{\partial x^2} - \frac{1}{c^2}\frac{\partial^2 w}{\partial t^2} - \eta\frac{\partial w}{\partial t} + \tilde{q}\right)dx\,dt = 0 \ . \tag{6.62}$$

Integrating (6.62) by parts with respect to x and t we obtain

$$\iint_\Omega v^*\frac{\partial v}{\partial t}\,d\Omega + \iint_\Omega \frac{\partial v^*}{\partial x}\frac{\partial w}{\partial x}\,d\Omega + \iint_\Omega \frac{\partial v^*}{\partial x}\varepsilon_0\,d\Omega - \eta\iint_\Omega v^*v\,d\Omega = 0 \ . \tag{6.63}$$

Here, ε_0 is the initial strain.

We assume a linear variation in velocity $v = \partial w / \partial t$ in terms of x and t:

$$v(x,t) = \sum_{i=1}^{4} N_i(x,t) v_i .$$
(6.64)

In the area of Ω, the shape functions $\mathbf{N} = [N_1, \ldots, N_4]$ have the form

$$N_1 = \frac{1}{bh}(x-b)(t-h) ,$$
$$N_2 = -\frac{1}{bh}x(t-h) ,$$
$$N_3 = -\frac{1}{bh}(x-b)t ,$$
$$N_4 = \frac{1}{bh}xt .$$
(6.65)

The displacements are determined by integration:

$$w(x,t) = w(x,0) + \int_0^t (N_1 v_1 + \ldots + N_4 v_4)\, dt .$$
(6.66)

The result is

$$w(x,t) = w(x,0) + \frac{xt^2}{2bh}(v_1 - v_2 - v_3 + v_4) + \frac{xt}{b}(-v_1 + v_2) + \frac{t^2}{2h}(-v_1 + v_3) + v_1 t .$$
(6.67)

The derivative $\partial w / \partial x$ is obtained from (6.67):

$$\frac{\partial w}{\partial x} = \frac{t^2}{2bh}(v_1 - v_2 - v_3 + v_4) + \frac{t}{b}(-v_1 + v_2) + \left.\frac{dw}{dx}\right|_{t=0} ,$$
(6.68)

where $\varepsilon_0 = dw/dx|_{t=0}$. It is essential to select the appropriate virtual velocity function. Following the derivation for the oscillator, we assume

$$v^*(x,t) = \delta(t - \alpha h)\left(\left(1 - \frac{x}{b}\right)v_3 + \frac{x}{b}v_4\right) .$$
(6.69)

Here, δ is the Dirac delta function. The required derivatives of the virtual function v^* and real function v are obtained from (6.69) and (6.64)

$$\frac{\partial v^*}{\partial x} = \frac{1}{b}(-v_3 + v_4) ,$$
(6.70)

$$\frac{\partial v}{\partial t} = \frac{x}{bh}(v_1 - v_2 - v_3 + v_4) + \frac{1}{h}(-v_1 + v_3) .$$
(6.71)

We note that due to the Dirac delta function part of the integrand, the integration over Ω is, in terms of x, reduced to an integration over the interval $[0, b]$. Taking

into account the above relationships, the final form of the equation (6.63) can be written in matrix form:

$$
\left\{ \rho A \int_0^b \begin{bmatrix} 0 \\ 0 \\ -(\frac{x}{b}-1) \\ \frac{x}{b} \end{bmatrix} \left[\frac{x}{bh} - \frac{1}{h}, \ -\frac{x}{bh}, \ -\frac{x}{bh}+\frac{1}{h}, \ \frac{x}{bh} \right] dx + \right.
$$

$$
+N \int_0^b \begin{bmatrix} 0 \\ 0 \\ -\frac{1}{b} \\ \frac{1}{b} \end{bmatrix} \left[\frac{t^2}{2bh} - \frac{t}{b}, \ -\frac{t^2}{2bh}+\frac{t}{b}, \ -\frac{t^2}{2bh}, \ \frac{t^2}{2bh} \right] dx \Bigg|_{t=\alpha h} -
$$

$$
-\eta \int_0^b \begin{bmatrix} 0 \\ 0 \\ -(\frac{x}{b}-1) \\ \frac{x}{b} \end{bmatrix} \left[\frac{(x-b)(t-h)}{bh}, \ -\frac{x(t-h)}{bh}, \ -\frac{(x-b)t}{bh}, \ \frac{xt}{bh} \right] dx \Bigg|_{t=\alpha h} +
$$

(6.72)

$$
\left. +N\,\varepsilon_0 \int_0^b \begin{bmatrix} 0 \\ 0 \\ -\frac{1}{b} \\ \frac{1}{b} \end{bmatrix} dx \right\} \cdot \left\{ \begin{array}{c} v_1 \\ \vdots \\ v_4 \end{array} \right\} = \mathbf{Q} \,.
$$

We see that the first two rows of all the matrix products are zero. From now on, we will operate only with the lower half of the matrix obtained after integration. The resulting matrices take the following form:

$$
\mathbf{M} = \frac{\rho A b}{h} \begin{bmatrix} -\frac{1}{3} & -\frac{1}{6} & \frac{1}{3} & \frac{1}{6} \\ -\frac{1}{6} & -\frac{1}{3} & \frac{1}{6} & \frac{1}{3} \end{bmatrix} = \frac{1}{h}\left[-\mathbf{M}_{stat} \mid \mathbf{M}_{stat}\right] \,, \tag{6.73}
$$

$$
\mathbf{K} = \frac{Nh}{b} \begin{bmatrix} \alpha(1-\frac{\alpha}{2}) & -\alpha(1-\frac{\alpha}{2}) & \frac{\alpha^2}{2} & -\frac{\alpha^2}{2} \\ -\alpha(1-\frac{\alpha}{2}) & \alpha(1-\frac{\alpha}{2}) & -\frac{\alpha^2}{2} & \frac{\alpha^2}{2} \end{bmatrix} =
$$

$$
= h\left[\alpha\left(1-\frac{\alpha}{2}\right)\mathbf{K}_{stat} \mid \frac{\alpha^2}{2}\mathbf{K}_{stat} \right] \,, \tag{6.74}
$$

$$
\mathbf{C} = \eta b \begin{bmatrix} \frac{1-\alpha}{3} & \frac{1-\alpha}{6} & \frac{\alpha}{3} & \frac{\alpha}{6} \\ \frac{1-\alpha}{6} & \frac{1-\alpha}{3} & \frac{\alpha}{6} & \frac{\alpha}{3} \end{bmatrix} = \left[(1-\alpha)\mathbf{C}_{stat} \mid \alpha\mathbf{C}_{stat}\right] \,, \tag{6.75}
$$

$$
\mathbf{e} = N\varepsilon_0 \left\{ \begin{array}{c} -1 \\ 1 \end{array} \right\} \,. \tag{6.76}
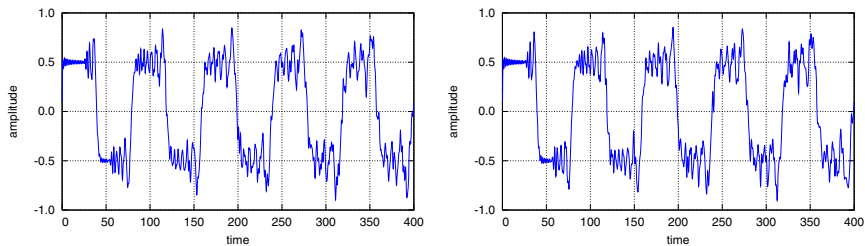$$

Fig. 6.12 Displacements of the free end of the bar, obtained by the space–time elements of the full matrix of mass coefficients at $\alpha = 0.5$ and $\alpha = 1.0$ at $\alpha = 0.5$ and $\alpha = 1.0$.

The final form of the equations of motion describes the balance of forces on the boundary of the domain Ω

$$(\mathbf{M} + \mathbf{C} + \mathbf{K}) \left\{ \begin{matrix} \dot{\mathbf{q}}_a \\ \dot{\mathbf{q}}_p \end{matrix} \right\} + \mathbf{e} = \mathbf{Q} \ . \tag{6.77}$$

The nodal velocity vector $\dot{\mathbf{q}}$ contains the velocities $\dot{\mathbf{q}}_a$ at the initial time $t = 0$ and $\dot{\mathbf{q}}_p$, those at the final time $t = h$. We get a matrix equation in which $\dot{\mathbf{q}}_p$ is the unknown. Figure 6.12 shows a graph of the axial displacement plotted over time at the free end of the rod, forced with the initial pulse. Figure 6.13 shows the result of an identical task, but using a diagonal inertia matrix.
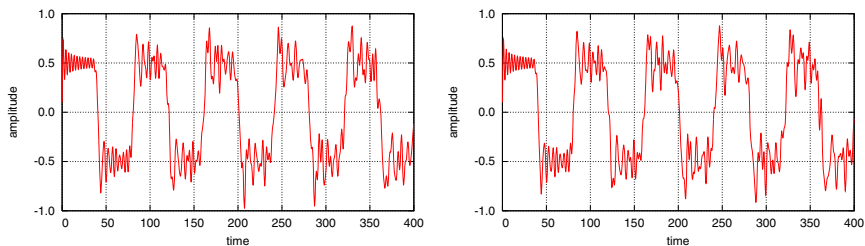

Fig. 6.13 Displacements of the free end of the bar obtained by the space–time element method with a diagonal mass matrix, for $\alpha = 0.5$ and $\alpha = 1.0$.

6.3.2.1 Example of a Vibrating String Loaded with a Moving Force

The diagram of the task (Figure 6.14) and the results for comparison are taken from [31]. The authors performed calculations using the methods of Fourier and of d'Alembert. Below, the same problem is solved by the with the velocity formulation of the space–time finite element method.

The following values were assumed: length of string $l = 100$ m, tension $T_0 = 10$ kN, mass density $\rho A = 0.89$ kg/m, point force $P_0 = 90$ N, concentrated mass $m = 10$ kg, damping $c_1 = c_2 = 0$. A conditionally stable variant of the method, with parameter $\alpha = 0.5$ and numerical damping $\gamma = 0.1$, was assumed.
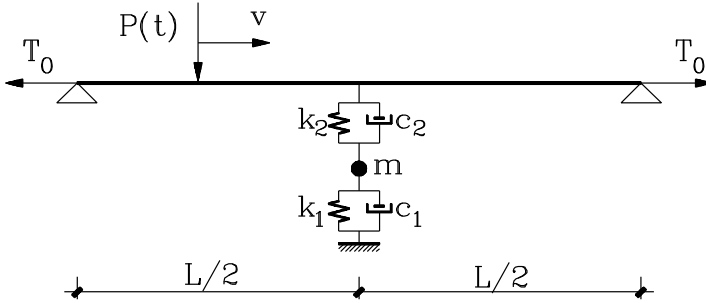
Fig. 6.14 String loaded by a moving force.

In the first case we assumed $m = c_1 = c_2 = 0$. The force $P(t) = P_0 \sin \omega t$ was harmonic with a frequency of $\omega = 0.4$ (this corresponds to 40 cycles over 200 m). The velocity v was 79.5 m/s (corresponding to $0.75c$). Figure 6.15 shows the lateral displacement at selected moments. The vertical lines on the first three graphs mark the position of the force. The thick line shows the results obtained by the space–time element method, and the thin lines those by the Fourier method. We can see a very good agreement of both solutions.

The second example is more complex. In the mid-span it includes a support consisting of two springs, k_1, k_2, and a mass m, which are non-zero. The force is constant and moves with the speed v $= 79.5$ m/s. Figure 6.16 presents the results, a thick vertical bar indicates a support. The solutions obtained using the space–time element method and the Fourier method coincide. In the cited paper [31], the results obtained by qualitatively different wave methods differ from both the results shown in Figure 6.16.
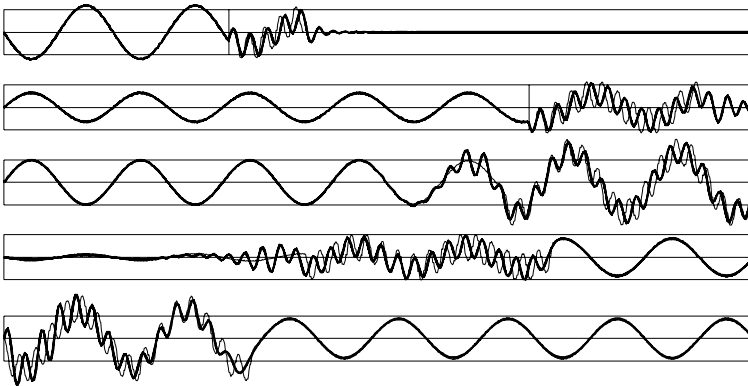

Fig. 6.15 Lateral displacements of the string at moments equal to 0.3, 0.7, 1.0, 1.2, and 1.5 of the total time of passage of the load (thin line: Fourier method, thick line: space–time element method).
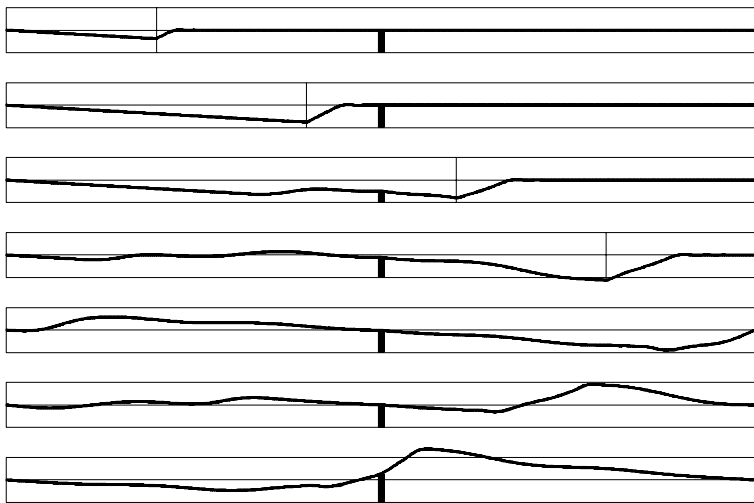
Fig. 6.16 Lateral displacements of the string at each 0.2 of the total time of passage of the load (thin line: Fourier method [32], thick line: space–time element method).

6.3.3 General Case of Elasticity

We now turn to a more general approach that allows the discretization of any dynamics problem of a continuous system.

If we define the deformations ε by

$$\varepsilon = \mathcal{D}\mathbf{w} , \tag{6.78}$$

where $\mathcal{D}$ is a differential operator, and the tension σ by

$$\sigma = \mathbf{E}\varepsilon , \tag{6.79}$$

and if we assume a certain distribution of virtual velocity $\mathbf{v}^*$, the equation of virtual work, expressed in terms of velocities, takes the following form

$$\int_{\Omega} (\mathbf{v}^*)^T \rho \frac{\partial \mathbf{v}}{\partial t} d\Omega + \int_{\Omega} (\dot{\varepsilon}^*)^T \sigma d\Omega + \int_{\Omega} (\mathbf{v}^*)^T \eta_z \mathbf{v} d\Omega = 0 . \tag{6.80}$$

The inertia of the system is given by the matrix ρ and the damping is described by η. The displacements $\mathbf{w}(t)$ are given by the integral

$$\mathbf{w}(t) = \mathbf{w}_0 + \int_0^t \mathbf{v} \, dt . \tag{6.81}$$

After taking into account (6.78), (6.79), and (6.81), we get

$$\int_{\Omega}(\mathbf{v}^*)^T\rho\frac{\partial\mathbf{v}}{\partial t}\mathrm{d}\Omega+\int_{\Omega}(\mathscr{D}\mathbf{v}^*)^T\mathbf{E}\underbrace{\mathscr{D}\mathbf{w}_0}_{\varepsilon_0}\mathrm{d}\Omega+\int_{\Omega}\left[(\mathscr{D}\mathbf{v}^*)^T\mathbf{E}\mathscr{D}\int_0^t\mathbf{v}\,\mathrm{d}t\right]\mathrm{d}\Omega+$$

$$+\int_{\Omega}(\mathbf{v}^*)^T\eta_z\mathbf{v}\,\mathrm{d}\Omega=0\,. \tag{6.82}$$

Now we introduce the interpolation formula

$$\mathbf{v}=\mathbf{N}\dot{\mathbf{q}}\quad\text{and}\quad\mathbf{v}^*=\mathbf{N}^*\dot{\mathbf{q}}\,. \tag{6.83}$$

Finally we have

$$\left\{\int_{\Omega}\left[(\mathscr{D}\mathbf{N}^*)^T\mathbf{E}\mathscr{D}\int_0^t\mathbf{N}\,\mathrm{d}t\right]\mathrm{d}\Omega+\int_{\Omega}(\mathbf{N}^*)^T\rho\frac{\partial\mathbf{N}}{\partial t}\mathrm{d}\Omega+\int_{\Omega}(\mathbf{N}^*)^T\eta_z\,\mathbf{N}\,\mathrm{d}\Omega\right\}\dot{\mathbf{q}}+$$

$$+\int_{\Omega}(\mathscr{D}\mathbf{N}^*)^T\mathbf{E}\varepsilon_0\,\mathrm{d}\Omega=\mathbf{0}\,. \tag{6.84}$$

We assumed before the distribution of virtual displacements depending on nodal parameters in which $t=h$. In such a case, the expression (6.84) has zeroes in the upper halves of the matrices $\mathbf{M}$, $\mathbf{K}$ and of the vector $\mathbf{e}$. As before, we can control the properties of the procedure by choosing the parameter α.

Concerning the cost of computing the resulting formula, we need to go back to the given virtual distributions of the nodal parameters. A Dirac distribution with respect to time reduces the problem of integration in the space–time element volume Ω to an integral on the surface which is the section in time $t=\alpha h$, in terms of spatial variables x,y,z. This reduces the calculational cost in comparison with the cost of the procedures obtained by the classical, linear interpolation of virtual parameters with respect to time.

In the case of (6.84), the areas of integration are reduced, from the space–time volume Ω to the space–time surface (real spatial domain) $V(\alpha h)$. The first integral contains a component integrated within the limits $[0,\alpha h]$. Due to the above conclusion concerning the integrals of the distribution, it is sufficient to integrate within the limits $[0,\alpha h]$. Assuming linearity of the integrands $\mathbf{N}$ we can determine the average value of the integrand at $t=\alpha h/2$ and multiply by the length of the interval αh. Then the stiffness, inertia, and damping matrices, and the initial stress vector describing the space–time element have the following forms:

$$\mathbf{K}=\int_{V_{\alpha h}}(\mathscr{D}\mathbf{N}_{\alpha h}(\mathbf{x}))^T\mathbf{E}\,\mathscr{D}\mathbf{N}(\mathbf{x},\alpha h/2)\,\mathrm{d}V\cdot\alpha h\,, \tag{6.85}$$

$$\mathbf{M}=\int_{V_{\alpha h}}\mathbf{N}_{\alpha h}^T(\mathbf{x})\rho\,\frac{\partial\mathbf{N}(\mathbf{x},\alpha h)}{\partial t}\,\mathrm{d}V\,, \tag{6.86}$$

$$\mathbf{Z}=\int_{V_{\alpha h}}\mathbf{N}_{\alpha h}^T(\mathbf{x})\,\eta_z\mathbf{N}(\mathbf{x},\alpha h)\,\mathrm{d}V\,, \tag{6.87}$$

$$\mathbf{e}=\int_{V_{\alpha h}}(\mathscr{D}\mathbf{N}_{\alpha h}(\mathbf{x}))^T\mathbf{E}\,\varepsilon_0\,\mathrm{d}V\,. \tag{6.88}$$

Here, $V_{\alpha h}$ is the element which is the cross-space at $t = \alpha h$, $\mathbf{N}_{\alpha h}$ is the matrix of the interpolated functions defined on the surface $V_{\alpha h}$, and $\mathbf{N}(\mathbf{x}, \cdot)$ is the matrix interpolation function in Ω established at a specific time. Changing the limits of integration makes the formula even simpler for numerical calculation of the characteristic matrices. The matrices (6.85), (6.86), and (6.87) have dimensions $N \times 2N$ (N is the total number of degrees of freedom). They bind together the time-moments t_i and t_{i+1}.

If the actual velocity distribution functions are linear, this formulation is approximately equivalent to the procedure previously discussed when $\alpha = 0.5$. Identical compounds are obtained for small deformations, when $\mathbf{x}_i = \mathbf{x}_{i+1}$. For large deformations the spatial geometry is taken at a time coinciding with the centre of gravity of the space–time element, and thus for positive deformations, i.e., extensions of the domain in time, above $\alpha = 0.5$, and for negative, below $\alpha = 0.5$.

6.3.4 Other Functions of the Virtual Velocity

The procedure here is the same as in the case of the virtual functions assumed according to (6.50). We review and examine the properties of different types of virtual functions. The accuracy and stability of the solution depend on the shape functions. In the following, we will give the stiffness and inertia matrices of the rod element obtained with different virtual functions. We will estimate the discretization error of the method [26].

6.3.4.1 Global Equilibrium (Hat Function)

We postulate a global equilibrium in the interval $[0, h]$. We assume a constant function (for example equal to 1) in the time interval (Figure 6.17a)

$$v^*(x,t) = \left(1 - \frac{x}{b}\right) v_3 + \frac{x}{b} v_4 . \tag{6.89}$$

The resulting stiffness and inertia matrices have the form

$$\mathbf{K} = \frac{EAh}{b} \left[\begin{array}{cc|cc} \frac{1}{3} & -\frac{1}{3} & \frac{1}{6} & -\frac{1}{6} \\ -\frac{1}{3} & \frac{1}{3} & -\frac{1}{6} & \frac{1}{6} \end{array} \right] , \tag{6.90}$$
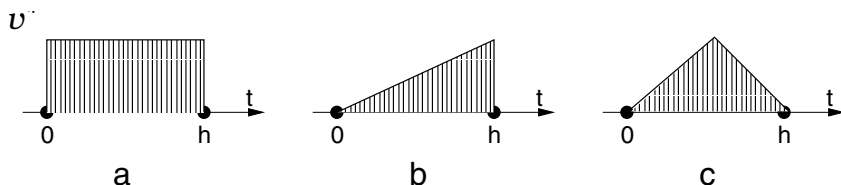

Fig. 6.17 Virtual functions: a – hat-type, b – triangular, c – roof-type.

$$\mathbf{M} = \frac{\rho A b}{h} \left[\begin{array}{cc|cc} -\frac{1}{3} & -\frac{1}{6} & \frac{1}{3} & \frac{1}{6} \\ -\frac{1}{6} & -\frac{1}{3} & \frac{1}{6} & \frac{1}{3} \end{array} \right] . \tag{6.91}$$

The displacements at the next point in time are determined based on the average speed rule $\mathbf{q}_{i+1} = \mathbf{q}_i + h(\mathbf{v}_i + \mathbf{v}_{i+1})/2$. In practice it is the expression (6.54) at $1/2 \leq \beta \leq 1$.

6.3.4.2   Triangular Function

In the interval $[0, h]$ we assume a virtual distribution time function in the shape of a triangle (Figure 6.17b)

$$v^*(x,t) = \left(1 - \frac{x}{b}\right) \frac{t}{h} v_3 + \frac{x}{b} \frac{t}{h} v_4 . \tag{6.92}$$

The stiffness and inertia matrices in this case have the form

$$\mathbf{K} = \frac{EAh}{b} \left[\begin{array}{cc|cc} \frac{5}{24} & -\frac{5}{24} & \frac{1}{8} & -\frac{1}{8} \\ -\frac{5}{24} & \frac{5}{24} & -\frac{1}{8} & \frac{1}{8} \end{array} \right] , \tag{6.93}$$

$$\mathbf{M} = \frac{\rho A b}{h} \left[\begin{array}{cc|cc} -\frac{1}{6} & -\frac{1}{12} & \frac{1}{6} & \frac{1}{12} \\ -\frac{1}{12} & -\frac{1}{6} & \frac{1}{12} & \frac{1}{6} \end{array} \right] . \tag{6.94}$$

From the condition of stability we obtain the parameter $2/3 \leq \beta \leq 1$.

6.3.4.3   Roof Function

In this case, we assume a distribution of the virtual time function in the shape of a double triangle as shown in Figure 6.17c

$$v^*(x,t) = \begin{cases} \left(1 - \frac{x}{b}\right) \frac{2t}{h} v_3 + \frac{x}{b} \frac{2t}{h} v_4, & \text{at } 0 \leq t \leq t/2 , \\ \left(1 - \frac{x}{b}\right)\left(-\frac{2t}{h} + 2\right) v_3 + \frac{x}{b}\left(-\frac{2t}{h} + 2\right) v_4, & \text{at } t/2 < t \leq h . \end{cases} \tag{6.95}$$

The stiffness and inertia matrices have in this case the form

$$\mathbf{K} = \frac{EAh}{b} \left[\begin{array}{cc|cc} \frac{17}{96} & -\frac{17}{96} & \frac{7}{96} & -\frac{7}{96} \\ -\frac{17}{96} & \frac{17}{96} & -\frac{7}{96} & \frac{7}{96} \end{array} \right] , \tag{6.96}$$

$$\mathbf{M} = \frac{\rho A b}{h} \left[\begin{array}{cc|cc} -\frac{1}{6} & -\frac{1}{12} & \frac{1}{6} & \frac{1}{12} \\ -\frac{1}{12} & -\frac{1}{6} & \frac{1}{12} & \frac{1}{6} \end{array} \right] . \tag{6.97}$$

The stability condition requires the parameter $3/4 \leq \beta \leq 1$.

6.3.4.4 Point Equilibrium

Using the Dirac delta function as the virtual velocity distribution was described in Chapter 6.3.1. We will analyse the process described by equation (6.56). The velocity and displacement can be developed in Taylor series:

$$
\begin{aligned}
v_{i+1} = & \left(1 - \alpha\omega^2 h^2 + \frac{1}{2}\alpha^3\omega^4 h^4 + \mathcal{O}(h^6)\right) v_i + \\
& + \left(-\omega^2 h + \frac{1}{2}\alpha^2\omega^4 h^3 + \mathcal{O}(h^5)\right) w_i ,
\end{aligned}
\tag{6.98}
$$
$$
\begin{aligned}
w_{i+1} = & \left(h - \omega^2 h^3 \alpha(1-\alpha) + \mathcal{O}(h^5)\right) v_i + \\
& + \left(1 - \omega^2 h^2(1-\alpha) + \frac{1}{2}\omega^4 h^4 \alpha^2(1-\alpha) + \mathcal{O}(h^6)\right) w_i .
\end{aligned}
$$

The parameter $\omega^2 = k/m$ is the square of the eigenfrequency. Considering the expansions of the trigonometric functions, we can estimate the error of the method. To do this we must take into account two cases of initial conditions: $v(0) = 0$, $w(0) = 1$ and $v(0) = 1$, $w(0) = 0$, and compare the results (6.98) with the exact expansions of the solutions. We then obtain the velocity error ε^v

$$
\varepsilon_{11}^v = \omega^2 h^2 \left(\alpha - \frac{1}{2}\right) + \omega^4 h^4 \left(\frac{1}{24} - \frac{\alpha^3}{2}\right) + \mathcal{O}(h^6) ,
\tag{6.99}
$$

$$
\varepsilon_{12}^v = \omega^4 h^3 \left(\frac{1}{6} - \frac{\alpha^2}{2}\right) + \mathcal{O}(h^5) ,
\tag{6.100}
$$

and displacements error ε^u

$$
\varepsilon_{21}^u = \omega^2 h^3 \left(\alpha(1-\alpha) - \frac{1}{6}\right) + \mathcal{O}(h^5) ,
\tag{6.101}
$$

$$
\varepsilon_{22}^u = \omega^2 h^2 \left(\frac{1}{2} - \alpha\right) + \omega^4 h^4 \left(\frac{1}{24} - \frac{\alpha^2}{2}(1-\alpha)\right) + \mathcal{O}(h^6) .
\tag{6.102}
$$

The lower indices indicate elements of the transition matrix (6.56). We see that when $\alpha = 1/2$, the second degree terms vanish. The error is in this case $1/12 \, h^3 + \mathcal{O}(h^4)$.

A similar error analysis can be carried out also in the case of the other virtual velocity functions, shown previously. Estimating this is left to the reader.

The results of the sample calculations are shown in Figure 6.18. The string is loaded by a force moving with constant speed. The graphs were plotted in the range of $0.1c$ to $1.0c$, for each tenth of the wave speed c. The vertical displacement at the point of the moving force and the vertical displacement in the centre of the string are depicted. We see that spurious vibrations occur in the case $v = 1.0c$. This is the extreme case since the force moves with the speed of the wave. In the remaining cases, all the plots practically coincide with the theoretical results.
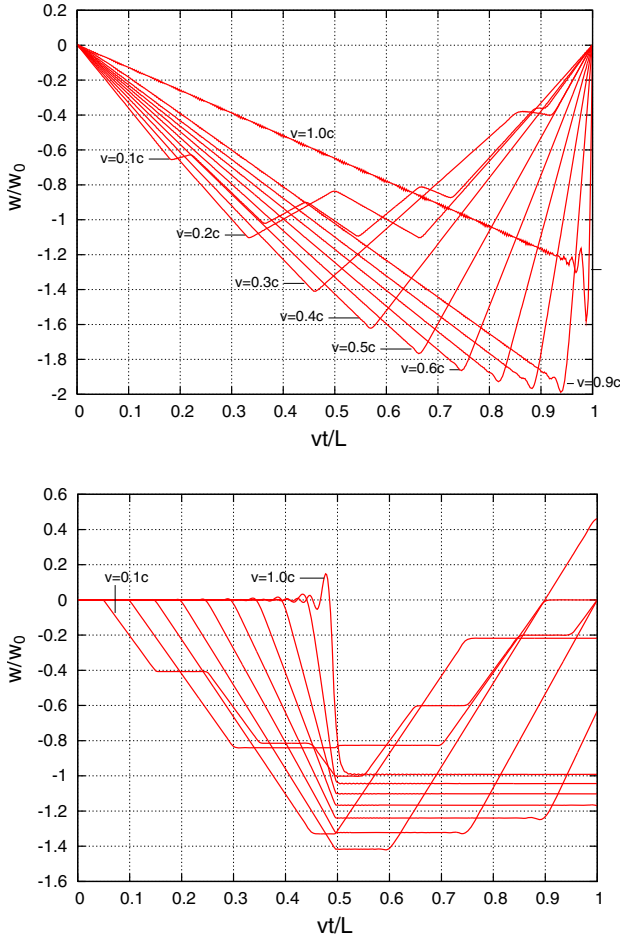
Fig. 6.18 Dimensionless displacements under the force (upper) and in the centre of the string (lower).

6.4 Space–Time Element Method and Other Time Integration Methods

6.4.1 Convergence

The error of the method is estimated as the difference between the exact and the approximate solution. The exact solution of the equation (6.47) is the sine wave $x = A \sin \omega t + B \cos \omega t$, with constants A and B derived from the initial conditions. Just subtract the development of our solution (6.56) from the exact solution developed in a Maclaurin series to determine the step error $[0, h]$. The case most preferred from the viewpoint of convergence is when $\alpha = 1/2$. The approximate solution converges to

Table 6.2 The convergence of the methods.

method	error degree	coefficient
s-t.e.m. $\alpha = 0$	Δt^2	$\frac{1}{2}$
s-t.e.m. $\alpha = \frac{1}{4}$	Δt^2	$\frac{1}{4}$
s-t.e.m. $\alpha = \frac{1}{2}$	Δt^3	$\frac{1}{12}$
s-t.e.m. $\alpha = \frac{\sqrt{2}}{2}$	Δt^2	$\frac{\sqrt{2}-1}{2}$
s-t.e.m. $\alpha = \frac{3}{4}$	Δt^2	$\frac{1}{4}$
s-t.e.m. $\alpha = 1$	Δt^2	$\frac{1}{2}$
s-t.e.m. $v^* = 1$ (6.104)	Δt^2	$\frac{1}{12}$
Runge–Kutta 2nd order	Δt^3	$\frac{1}{6}$
Runge–Kutta 4th order	Δt^5	$\frac{1}{120}$

the exact solution with an error proportional to the third power of the step Δt. Table 6.2 summarizes the different variants of the method. Using a linear combination of these variants defined with different α allows of improving the accuracy. Using virtual functions of the form $\sum_j \chi_j \delta(t/h - \alpha_j)$, where the α_j are the coordinates of the peaks, and χ_j the size (weight) of these peaks, the speed v_{i+1} is determined by

$$v_{i+1} = \frac{\sum_j \left(1 - \frac{kh^2}{2m}\left[1 - (1 - \alpha_j)^2\right]\right)\chi_j}{\sum_j \left(1 + \frac{kh^2 \alpha_j^2}{2m}\right)\chi_j} v_i - \frac{\frac{k}{m}h}{\sum_j \left(1 + \frac{kh^2 \alpha_j^2}{2m}\right)\chi_j} x_i . \qquad (6.103)$$

If we take $\alpha_1 = 0$, $\alpha_2 = 1/2$, and $\alpha_3 = 1$, then we obtain the appropriate coefficients χ_j: $\chi_1 = 1/6$, $\chi_2 = 2/3$, $\chi_3 = 1/6$. The solution has an error $\mathcal{O}(h^4)$ (exactly $h^4/12 + \mathcal{O}(h^5)$). Choosing the location of successive peaks we can reset more terms describing the local solution error. In this way we can construct a system of algebraic equations in which the unknowns will be shares of Dirac peaks in the final function of the virtual velocity. Another problem is the selection of the location α_i in the function $\delta(t - \alpha_i h)$. This can be done optimally, reducing the error and yet enabling the meeting of a specific criterion for the resulting factors (e.g. that they have equal sign). This issue will not be further dealt with here.

In a similar manner as in Chapter 6.3.1, one can define a family of computational schemes, differing in the shape of the virtual function adopted on exit, and thus differing in the points where equilibrium is established. Yet noteworthy is the scheme expressing the global equilibrium, when the speed of a virtual function is equal to unity throughout the period of time h, except for the ends of the interval, where the values are zero. The resulting formula is the following:

$$v_{i+1} = \frac{1 - \frac{k}{m}\frac{h^2}{3}}{1 + \frac{k}{m}\frac{h^2}{6}} v_i - \frac{\frac{k}{m}h}{1 + \frac{k}{m}\frac{h^2}{6}} x_i, \quad x_{i+1} = x_i + \frac{1}{2}h(v_i + v_{i+1}). \tag{6.104}$$

The scheme (6.104) has a local error of $\mathcal{O}(h^3)$ (exactly $h^3/12$) and is conditionally stable. The stability condition imposes in this case the restriction $\omega h \le 2\sqrt{3}$.

The operators a_1 of the difference formula $y_{i+1} = a_1 y_i + a_2 y_{i-1}$ for the selected methods are presented in Table 6.3. a_2 is equal to minus one. Figure 6.19 illustrates the phase error of the chosen methods of integration of the differential equation of motion: the space-time element method (STEM), displacement formulation, with the parameter η, the space-time element method, velocity formulation, with the parameter α, the Newmark method (NM), and the trapezoidal method (TM). It can be shown that when $\alpha = \sqrt{2\beta}$ (where β is the parameter of the Newmark method) the scheme (6.56) corresponds to the Newmark method. It should be noted that the identity of the Newmark method and the space–time element method is limited to the case of a zero damping matrix. In general, a full analogy has so far failed to show.

Table 6.3 Operators of the difference schemes of the integration of the differential equation.

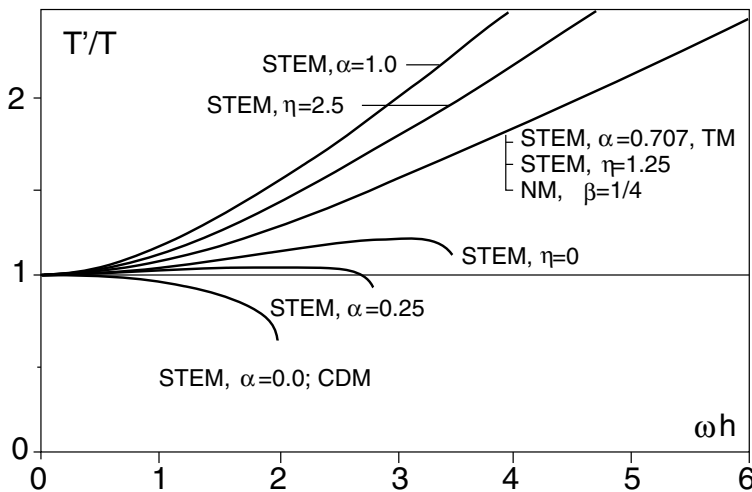| method		operator
central difference m.		$2 - \kappa$
trapezoidal m.		$\frac{2(4-\kappa)}{4+\kappa}$
Newmark m.:	$\beta=1/4, \gamma=1/2$	$\frac{2(4-\kappa)}{4+\kappa}$
	$\beta=1/6, \gamma=1/2$	$\frac{4(3-\kappa)}{6+\kappa}$
	$\beta=1/12, \gamma=1/2$	$\frac{2(12-5\kappa)}{12+\kappa}$
	$\beta=0, \gamma=1/2$	$2 - \kappa$
STEM—displacement formula: classical ($\eta=0$)		$\frac{4(3-\kappa)}{6+\kappa}$
	$\eta=5/4$	$\frac{2(4-\kappa)}{4+\kappa}$
	$\eta=5/2$	$\frac{6-\kappa}{3+\kappa}$
STEM—velocity formula:	$\alpha=0$	$2 - \kappa$
	$\alpha=1/2$	$\frac{16-6\kappa}{8+\kappa}$
	$\alpha=\sqrt{2}/2$	$\frac{2(4-\kappa)}{4+\kappa}$
	$\alpha=1$	$\frac{4}{2+\kappa}$
	formula with $v^*=1$ (6.104)	$\frac{4(3-\kappa)}{6+\kappa}$

Fig. 6.19 The phase error of the time integration methods: CDM – central difference method, NM – Newmark method, TM – trapezoidal method, STEM – space–time element method.

6.4.2 Phase Error

The phase error in the integration scheme expressed in velocities is determined by the ratio

$$P = \frac{T'}{T} = \frac{\omega}{\omega'} . \tag{6.105}$$

The characteristic equation of the scheme described by (6.56) has the form

$$\lambda^2 - (T_{11} + T_{22})\lambda + (T_{12}T_{21} - T_{11}T_{22}) = 0 , \tag{6.106}$$

where T_{ij} are the elements of the transition matrix (6.56). The solution of (6.106) gives

$$\lambda_{1/2} = \frac{\alpha^2 \kappa + 2 - \kappa \pm i\sqrt{\kappa(2\alpha^2\kappa + 4 - \kappa)}}{\alpha^2 \kappa + 2}, \quad \kappa = \frac{k}{m}h^2 . \tag{6.107}$$

Since the frequency in the numerical scheme is determined by

$$\text{tg}\,\omega'h = \frac{\Im(\lambda)}{\Re(\lambda)}, \quad \omega' = \frac{1}{h}\text{arctg}\frac{\Im(\lambda)}{\Re(\lambda)} , \tag{6.108}$$

the phase error is

$$P = \frac{\sqrt{\kappa}}{\text{arctg}\left(\frac{\sqrt{\kappa(2\alpha^2\kappa+4-\kappa)}}{\alpha^2\kappa+2-\kappa}\right)} , \tag{6.109}$$

and in the limit

$$\lim_{\kappa \to 0} P = 0 . \tag{6.110}$$

■

There remains the question, which variant of the method, explicit or implicit, should be adopted in computations? The following is a summary which partially characterizes the basic features of both these groups.

Implicit methods

- Implicit methods are usually unconditionally stable. The size of the time step depends only on the required accuracy.
- The calculations require a greater number of arithmetic operations per one computational step, and more memory.
- The precision criteria require that the time step be approximately one hundredth of the basic period of oscillation.
- The algorithms require the decomposition of the matrix into factors (factorization).
- Implicit methods are convenient in the analysis of inertial issues.
- Implicit methods are recommended for bent structures due to the high value of the highest vibration frequency compared to the basic period.
- The efficiency of this group of methods is lower in the analysis of multidimensional systems.

Explicit methods

- Stability conditions limit the time step of explicit methods.
- Calculations are effective with diagonal mass matrices. Consistent mass matrix improves the accuracy of bent structures but overestimates the frequency, while a diagonal matrix lowers the frequency. A diagonal modified matrix [66] (when the total mass of the finite element is distributed on the diagonal elements with the ratio of the consistent matrix) has the most advantageous properties.

6.4.3 Non-inertial Problems

Now let us look at the solution of massless tasks. We will apply the space–time element method. We will consider in fact static problems, although the process of material deformation is kinematically induced. This way we can obtain illustrative results for quasistatic deformation processes. We can apply this approach to the material shaping processes in forms, car stringers crushing, etc.

Let us examine the stability of the solution scheme based on the velocity space–time element method with zero inertia coefficients. In this scheme we use the Dirac delta function for the virtual speed. Assuming $m = 0$, we calculate the moduli of the eigenvalues of the transition matrix $\mathbf{T}$ for the problem of a single degree of freedom. Figure 6.20 shows the dependence of the two eigenvalues on the value of the parameter α for the massive and the massless tasks. In the case of an inertial system, the modulus of an eigenvalue does not exceed 1 when $\alpha \geq \sqrt{2}/2$. In non-inertial problems, the moduli of both eigenvalues are equal to 1 only when $\alpha = 1$.
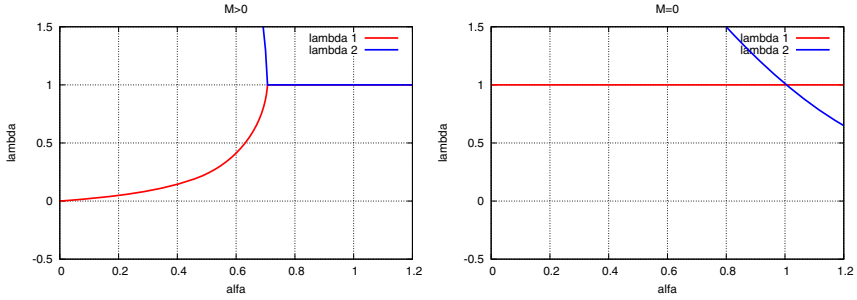
Fig. 6.20 Eigenvalues of the transition matrix for the massive ($m > 0$) and massless ($m = 0$) tasks.
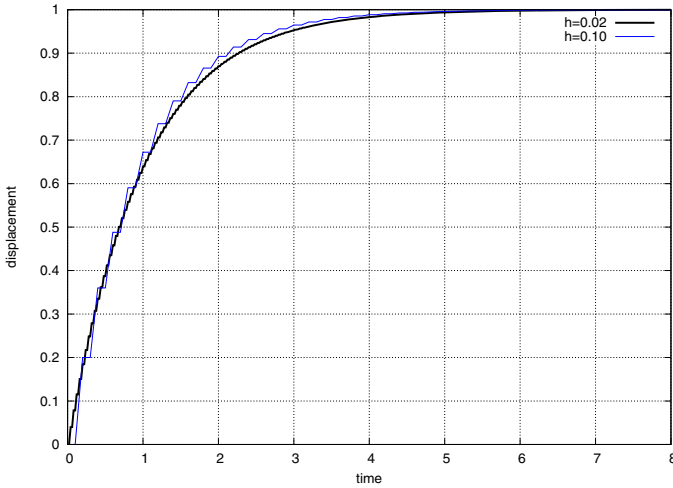

Fig. 6.21 Solution process for the massless spring subjected to a constant force, with time steps $h = 0.02$ and 0.1.

This is the only parameter of the procedure for which the solution is unconditionally stable when $m = 0$.

The space–time scheme applied to massless systems is advantageous since the same code can be applied both to inertial and non-inertial structures. Without needing reprogramming, the quasi-static problem can be transformed into a dynamic one. Below, the massless algorithm will be applied with the aim of comparing the numerical results for simple statical or quasi-statical problems. Let us look at the example.

Example 6.1. Let us consider an oscillator with zero mass. In practice, we consider a simple massless spring with stiffness $k = 1$, subjected to a force $P = -1$. All initial parameters, i.e., the velocity and displacement, are equal to zero. The system has

one degree of freedom. We can write the equilibrium equation with formulas for displacement x_{i+1} and nodal force e_{i+1}

$$
\begin{aligned}
&\left[\alpha\left(1-\frac{\alpha}{2}\right)v_i+\frac{\alpha^2}{2}v_{i+1}\right]+e_i = P_i\,,\\
&x_{i+1} = x_i+[\alpha v_i+(1-\alpha)v_{i+1}]h\,,\\
&e_{i+1} = x_{i+1}\,.
\end{aligned}
\tag{6.111}
$$

The results for $\alpha = 1$ are presented in Figure 6.21. Other values of α, lower than one, involve divergence of the time stepping process. We can notice that the computed displacement converges to the exact value, equal to one.

6.5   Space–Time Finite Element Method vs. Newmark Method

We link the vector composed of velocities and displacements at the next time with the same vector at the present time. We will deal with the simplified case. Assuming a zero value for the load function and a lack of damping, we will consider free undamped vibrations. Using Algorithm 5 after appropriate transformations we can write the transition matrix for the Newmark method

$$
\mathbf{T} = \begin{bmatrix}
\frac{1}{2\beta(h^2\omega^2\beta+1)}-\frac{1}{2\beta}+1 & -\frac{h\omega^2(h^2\omega^2(4\beta-1)+4)}{4(h^2\omega^2\beta+1)}\\[2mm]
\frac{h}{1+h^2\omega^2\beta} & \frac{1-h^2\omega^2(\frac{1}{2}-\beta)}{1+h^2\omega^2\beta}
\end{bmatrix}.
\tag{6.112}
$$

If we expand the terms of the matrix (6.112) into Taylor series and act similarly to the matrix (6.56), then for the parameter $\alpha = 1/2$ in the space–time element method and for $\beta = 1/2$ we obtain the compatibility of both matrices with the error level $\Delta\mathbf{T}$ of the range $\mathcal{O}(h^3)$

$$
\Delta\mathbf{T} = \begin{bmatrix}
0 & \frac{h^3\omega^4}{8}\\[2mm]
-\frac{h^3\omega^2}{4} & 0
\end{bmatrix}.
\tag{6.113}
$$

Only in the case of the application of the virtual hat function, and $\mathbf{C} = \mathbf{0}$, can one easily compare the Newmark method with the space–time element method and see their identity. We obtain the transition matrix of the space–time element method in the form (6.104). We then easily see that both arrays (6.104) and (6.112) are equal if $\beta = 1/6$ and $\gamma = 1/2$ in the Newmark method. Therefore, unless we take into account a damping described by the damping matrix $\mathbf{C}$, we obtain the identity of both methods.

Identical considerations hold for comparing the central difference method with the method of trapezoids. They are a particular case of the group of Newmark methods.

6.6   Simplex Elements

The diagrams of finite element solutions reduce to systems of algebraic equations. Their solution has a large share in the cost of the whole process of calculation. The number of arithmetic operations increases significantly in non-linear tasks that require multiple solving of the system of equations at each time step. There are two groups of methods for solving systems of equations: direct and iterative. The first one leads to a solution with a single engagement of the matrix coefficients. The matrix can be split into a product of two triangular matrices, or directly triangularized. The calculation of the unknowns in the system with the triangular matrix is immediate. We can use the classical decomposition LU on the matrix product of lower and upper triangular matrices, the Cholesky–Banachiewicz decomposition $U^T U$ on the product of a triangular matrix and its transposed form, the decomposition of Doolittle or LU Croute with ones on the diagonal of the matrix L or U and decomposition LDL^T, with the diagonal matrix D and the lower triangular matrix L. These methods are characterized by relatively low computational cost. The decomposition LDL^T and the Croute and Doolittle decomposition require $n^3/6$ multiplications, and the Gaussian decomposition requires $n^3/3$ operations. The computational cost in a real practical case depends on the bandwidth of the coefficient matrix of the system of equations. The disadvantage of the group of matrix decomposition methods is the need to first use special algorithms to reduce the bandwidth of the matrix. In the case of two-dimensional problems discretized with a mesh with the same number of nodes in both directions, the cost of the solution is proportional to the fourth power of the number of nodes in one direction of the grid. And in the case of a three-dimensional cube-shaped domain, covered with a mesh evenly in three directions, this cost increases with the seventh power of the number of nodes on one edge. Nonlinear effects and the need for iteration, slowed by an increase in the number of nodes, achieving the balance of forces, prolongs even more the computational process.

The second group, a group of iterative methods (e.g., Jacobi, Gauss–Jordan), rarely used in practice, allows the incorporation of nonlinear effects of the task into an iterative solving process. In this way, the approach to the solution is based on simultaneously updated matrix elements. This process can be carried out without forming a global matrix (or even part of it). This is the procedure performed 'element by element'. Although these are undoubtedly advantageous features, the whole computation process is very expensive and vulnerable to problems with its convergence and stability.

Another group of iterative methods of the 'element by element' type are presented, e.g., in the papers [68]. Their computational cost, however, is large and methods of this type start to be attractive only in sufficiently large tasks. Their convergence is relatively slow and depends on the conditioning of the matrix (and thus the bandwidth of the matrix, the shape of the test object, and the material parameters of the elements). It was concluded that they had a high sensitivity to nonlinear effects. The increase of the time step in nonlinear tasks worsens the convergence dramatically.
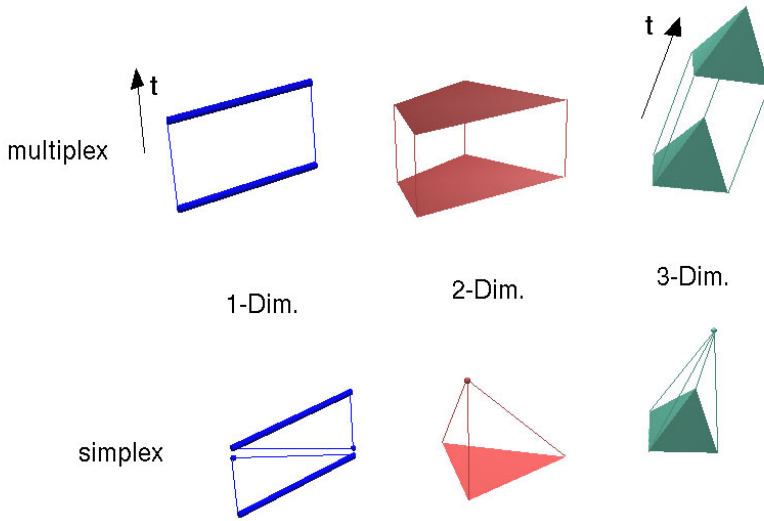
Fig. 6.22 Examples of multiplex and simplex elements of one-, two-, and three-dimensional objects.

The above drawbacks and particularly the difficulty in predicting the rate of convergence of iterative methods make direct methods more likely to be applied in practice.

The space–time approximation opens up new opportunities by applying simplicial space–time subdomains (Figure 6.22). These elements in one-dimensional real space and in time have the shapes of triangles. The elements of this shape can model axially vibrating rods, bending rods, or strings. Two-dimensional objects such as discs, plates, and shells in space are discretized with triangular spatial elements, and in time–space tetrahedra, created from these triangles. Three-dimensional blocks in space translate into hyper-tetrahedral simplices in time-space. Hyper-tetrahedra are creations in the $n+1$ dimensional space, and have $5-i$ $(i=1,\ldots,4)$ nodes in time t_i and i nodes in time t_{i+1}.

6.6.1 *Property of Space Division*

A space–time layer bounded by planes t_i and t_{i+1} can be filled with simplicial elements in many ways. The special filling of the space–time layer with simplices allows of gaining a triangular coefficient matrix for the system of equations directly in forming the global matrix (Figure 6.23). The creation of a space partition by triangles should be guided by the principle that skew edges run from the point $(x_i, \Delta t)$ to the point $(x_j, 0)$, if $i < j$. In this way, we obtain skew edges in time-space. Otherwise, i.e., $i \geq j$, we obtain the edges parallel to the time axis. We proceed similarly in a task of higher spatial dimensionality. The procedure is described in
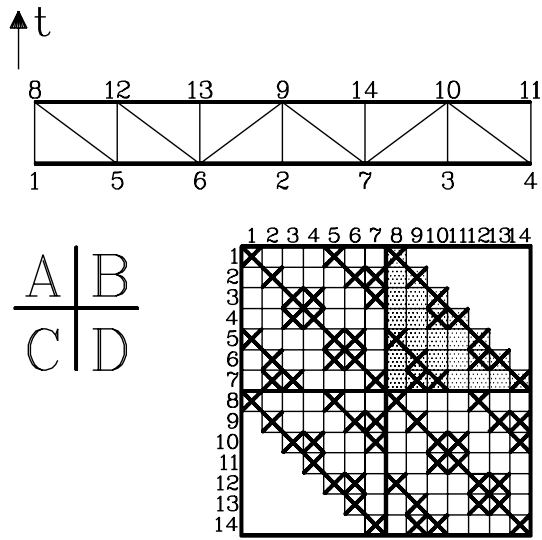
Fig. 6.23 Filling up the global matrix in the one-dimensional domain with a triangular grid of space–time elements.
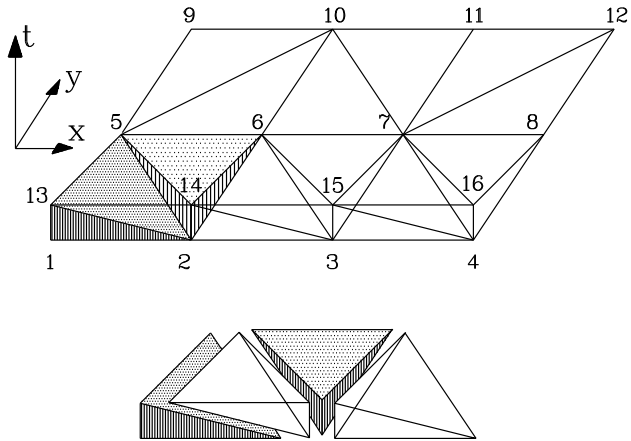

Fig. 6.24 Filling in the two-dimensional time-space.

Algorithm 10. The example of filling the volume of the space–time layer in a one-dimensional task is shown in Figure 6.24. In this way, a lower triangular matrix of coefficients is obtained.

In the same way, we create a layer of tetrahedral elements in two-dimensional spatial areas. This is illustrated in Figure 6.24. We can also obtain an upper triangular matrix of coefficients. When creating the space–time grid and constructing

---

Algorithm 10. The method of partitioning the time-space into simplex-shaped elements.

---

1. We consider successive nodes of the mesh of the space–time partition (for example node i).
2. We number the nodes of spatial elements which are in topological contact with the node considered:

   - if the number of the node of the element surrounding node i is greater than i, then the time coordinate of the new space–time node is equal to 0,
   - if the number of the node surrounding node i is smaller than i, then the time coordinate in the new space–time node is equal to h,
   - if it is the node i, then two nodes of the space–time element are created with the coordinates 0 and h.

---

the matrix of coefficients, we should proceed oppositely to Algorithm 10. We can extend the principle of filling the space–time layer with simplex elements by the following statement: any partition of the space–time layer with simplicial elements enables solving the resulting system of equations node by node. This should be done by choosing the appropriate sequence of nodes resulting from the method of filling the space–time layer with elements. This is obvious because the reordering of equations and variables in the vector of unknowns always brings such a system of equations to triangular form (upper or lower).

Solving the system of equations with a triangular matrix of coefficients is effective because we can proceed directly to solving it equation after equation. The characteristic property of such a procedure can be underlined. Is the flow of information in time in one spatial direction only: from the first equation to the last, i.e., from the spatial point associated with the first degree of freedom to the spatial point governed by the last degree of freedom in the system of algebraic equations (or vice versa, if we are dealing with an upper triangular matrix). In the time stepping process it is expressed in this way: the flow of information between the nodes of the spatial grid in one direction has a limited speed, but is unlimited in the opposite direction (Figure 6.25a). Numerical tests have shown that in the initial phase of the calculation, some differences in the results are observed. In the long term simulation, these differences are dominated by the errors arising from the discrete model, properties of the method of calculation of parasitic vibrations. Space–time anisotropy affects the performance of wave problems (shock, reflections, etc.). There is no significant effect of anisotropy on the results of the structural dynamics. An anisotropy can be removed by introducing a special division of the layer, without preference for any direction (Figure 6.25b).

Another practical property of having simplices for elements is the possibility of separating the parts of the system of equations. It allows sub-dividing the construction into substructures and solving the system of equations in separate batches. The whole structure, with the exception of nodes common to neighbouring substructures, can be modelled with elements of 'multiplex' type, and so in the classical
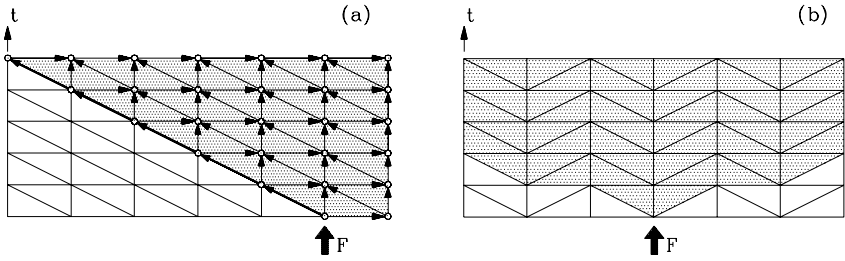
Fig. 6.25 Limit of the speed of information flow *(a)* and isotropic properties of time-space *(b)*.

way. Only elements connecting substructures should be simplicial (Figure 6.26). The solution is obtained in two stages: first the subsystem No. I is solved and then using the known solution in the node at the junction of two subdivisions is subsystem No. II solved. Thanks to this, the calculation can be carried out on parallel processors. Figure 6.27 shows for the example of the simplest element mesh, how the computational process can be divided between four processors. Their areas of involvement are outlined. Starting from the node nearest the origin of the coordinate system, we can move with time, carrying out calculations for the selected subsystems of elements. A larger number of processors allows even greater acceleration of the computational process.
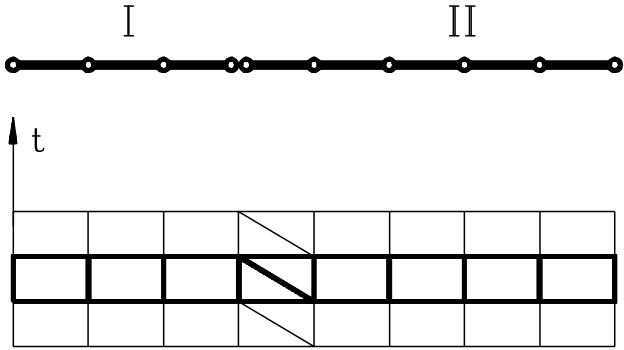

Fig. 6.26 The division of the domain into sub-areas using simplices.

The elements of higher order, with intermediate nodes both along the *x*-axis and the *t*-axis, also allow us to construct a system of equations which can be solved 'node after node'. This means that we can separate groups of nodes (Figure 6.28) that enter into the calculations sequentially. In this way, properties similar to the basic, low order elements are achieved, where the nodes are taken into the computations individually.
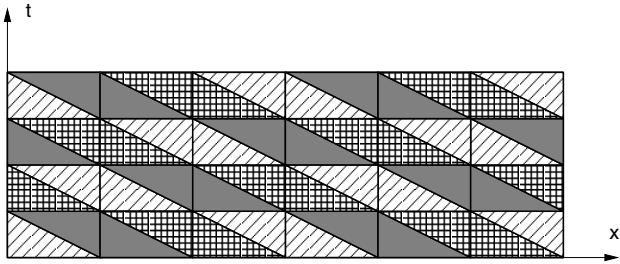
Fig. 6.27 Areas of activity of individual processors in a multiprocessor solution.
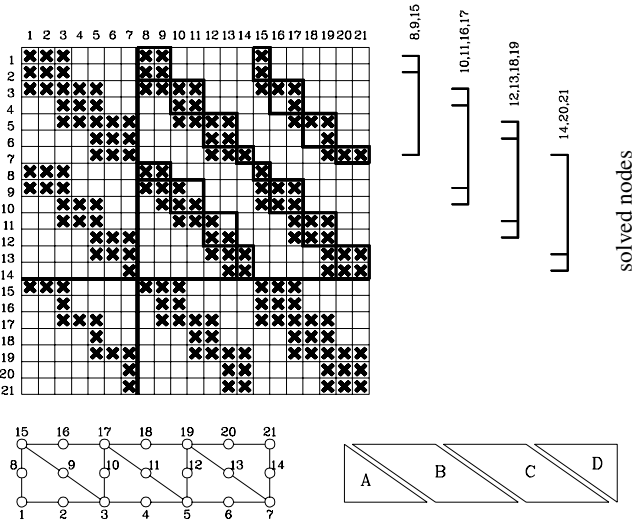

Fig. 6.28 Constructing and solving the system of equations for higher order space–time elements.

Another kind of division of the time-space is proposed in the papers [80, 114]. The nodes are arranged alternately every second time (Figure 6.29). The advantage of this approach is its lengthening of the integration step (although the stability of such a scheme has not yet been fully explored), isotropy, and above all decomposition of the system of equations. This helps reduce the number of iterative processes (such as at material nonlinearities) to each node, without having to manipulate entire arrays. A major drawback is the difficulty in practically applying such a division. Problems arise in covering even simple flat areas with such elements. At the edges and corners of the area we need to build three-dimensional objects of unusual shape, differing from the rest of the grid. The amount of work in the programming phase is so large that it can be profitable only for repeatedly performed structural calculations for huge meshes.
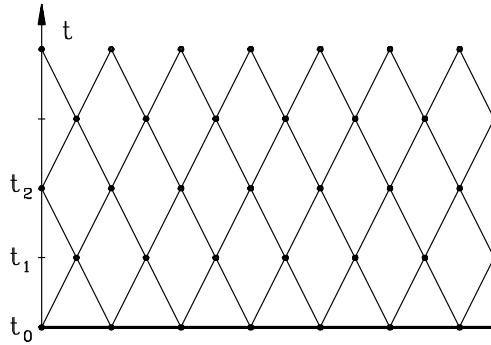
Fig. 6.29 Staggered arrangement of the element nodes.

6.6.2   Numerical Efficiency

Numerical efficiency is one of basic features that should be sought for when solving non-linear problems. Finding solutions in a single computational step consists of two phases: building the global matrix of coefficients, with prior modification of the geometric and material properties, and solving the algebraic equations. The computational cost of the process of integrating the equations of motion is significantly affected by the form of the matrix of inertia and the damping. A diagonal inertia matrix and numerical damping, described by a combination of stiffness and inertia matrix, allows shortening and simplifying the computations. The use of explicit integration schemes in time results in decoupling the system of equations. However, in some cases, consistent mass and damping matrices are required. In such cases, the need to solve the full system of equations raises the cost significantly.

The simplest assessment of the quality of the algorithm is to estimate the number of arithmetic operations necessary to carry out the calculation in one step. It can be assumed that the share of operations of multiplication M in the total number of arithmetic operations is constant. In the space–time element method the number of multiplications needed to solve the system of equations (not including the setting up the coefficients of the system) depends on the amount of memory used for collecting the coefficients. It is

$$M = 2sN(c+1) \tag{6.114}$$

if we engage $3.5sN(c+1)+1.5sN$ memory units, and it is

$$M = 3sN(c+1) \tag{6.115}$$

if we engage $1.5sN(c+1)+1.5sN$ memory units. By memory unit, we mean that portion of memory that stores a real number. By c we denote the number of nodes adjacent to a single node in the mesh, N denotes the total number of degrees of freedom, and s denotes the number of nodal degrees of freedom.

Comparing the full cost of computing one step in the space–time element method and in the finite element method combined with the method of central differences requires making certain assumptions. In the finite element method and in the central difference method we assumed

- creating a matrix of coefficients at each computing step,
- symmetry of the element matrices and the global matrix,
- regular band edge of the global matrix (filled with zeros),
- consistent inertia matrix,
- negligible damping (zero damping matrix),
- optimal numbering of the nodes to narrow the bandwidth of the matrix in the finite element method,
- perform multiplications by zero within the band,
- plane stress/strain elastic task as a model task adopted in estimation.

The comparison of the cost calculations is shown in Figure 6.30. We can compare the above estimates, (6.114) and (6.115), with [102]. The Newmark method requires $M = Nb^2/2n + N(4b + 3)$ multiplications per one step of calculations (where n is the number of time steps and b is the width of the half band). The Trujillo method [102, 139] for a matrix stored in band form requires $M = N(4b + 6)$ operations, and for storage in block form, $M = 2sN(c + 1) + 10N$. A summary of the computational cost of each method is given in Table 6.4. It should be noted that the width of the matrix half band b is usually proportional to $N^{1/2}$ in plane tasks and to $N^{1/3}$ in three-dimensional tasks. In the comparison, the entire group of methods using diagonal matrices of inertia and damping were omitted. They give decoupled equations and the cost of solving is then low.
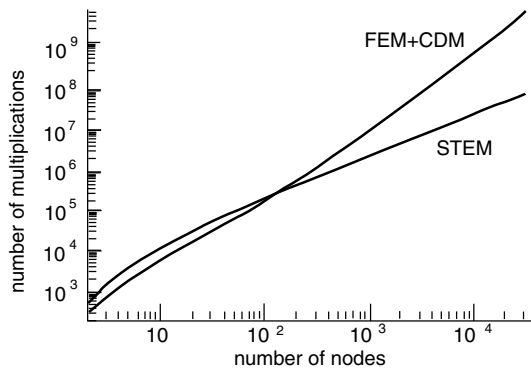

Fig. 6.30 Comparison of computational costs of the finite element method and the method of central differences with the space–time element method.

Table 6.4 Computational cost of numerical methods.

method	number of multiplications
Gauss m. (symmetric matrices)	$\frac{N^3}{6} + \frac{N^2}{4} + \frac{N}{12}$
Gauss m. (symmetric and band matrices)	$\frac{1}{2}b^2N$
STEM (higher memory)	$2sN(c+1)$
STEM (lower memory)	$3sN(c+1)$
Newmark m. [102]	$4bN + 3N$
Trujillo m. (with half band) [102]	$4bN + 6N$
Trujillo m. (with block notation) [102]	$2bN + 10N$

Conclusions

- The computational cost of the space–time element method grows linearly with the number of grid nodes.
- The number of operations in the space–time element method does not depend on the method of numbering the nodes (mesh topology).
- In classical methods, the half band width b increases with the size of the task. The number of arithmetic operations per one time step is then proportional to $bN \approx N^{3/2}$.
- Estimates are rough and may vary considerably for different specific tasks.

6.7 Simplex Elements in the Displacement Description

In the following sections we will derive the stiffness, inertia, and damping matrices of the basic simplicial space–time finite elements. We will deal with a rod or string element, the element of a beam of medium thickness, the slab, and a plate of medium thickness and three-dimensional body. The way to build a matrix is simple. We use the well-known procedure from the finite element method. The only difference is the inclusion of time as an additional coordinate of the coordinate system in which we describe a discrete element.

6.7.1 Triangular Element of a Bar Vibrating Axially

We use a linear displacement distribution inside the triangular element

$$w(x,t) = a_1x + a_2t + a_3 , \tag{6.116}$$

where a_1, a_2, a_3 are constants dependent on the geometry of the element and the values of the nodal displacements. It can be written in another way in surface coordinates L_i

$$w = L_1 u_1 + L_2 u_2 + L_3 u_3 , \tag{6.117}$$

where

$$L_i = \frac{1}{2\Delta} \det \begin{bmatrix} x & t & 1 \\ x_k & t_k & 1 \\ x_l & t_l & 1 \end{bmatrix} , \tag{6.118}$$

where i, k, l and j, m, n are the permutations of the numbers of the vertices in the triangle, and Δ is the surface area of a triangle.

The shape functions $N_i(x,t)$ are directly expressed by coordinates L_i

$$\mathbf{N} = [L_1, L_2, L_3] . \tag{6.119}$$

The differential operator can be considered as a matrix containing a single element $\mathscr{D} = \partial/\partial x$. If we take the origin to be the centre of gravity of the triangle, the stiffness $\mathbf{K}$ and inertia $\mathbf{M}$ matrices are

$$K_{ij} = \frac{EA}{4\Delta}(t_k - t_l)(t_m - t_n) , \tag{6.120}$$

$$M_{ij} = -\frac{\rho A}{4\Delta}(x_k - x_l)(x_m - x_n) . \tag{6.121}$$

The external damping $\mathbf{Z}$ has the form

$$Z_{ij} = \frac{\eta_z}{4\Delta}(x_k t_l - x_l t_k)(x_n - x_m) , \tag{6.122}$$

and the internal, due to the double differentiation of (6.116), is equal to zero.

6.7.2 Space–Time Finite Element of the Beam of Moderate Height

In a beam of moderate height, we take into account the effects of shear. Both the deflection w and the rotation θ are expressed by independent linear functions

$$\begin{Bmatrix} w \\ \theta \end{Bmatrix} = \begin{Bmatrix} a_1 x + a_2 t + a_3 \\ b_1 x + b_2 t + b_3 \end{Bmatrix} . \tag{6.123}$$

The coefficients a_i and b_i depend on the geometry of the space–time element. In surface coordinates L_1, L_2, and L_3, we can write the dependencies of the displacements on the nodal values:

$$\left\{ \begin{matrix} w \\ \theta \end{matrix} \right\} = \left\{ \begin{matrix} L_1 w_1 + L_2 w_2 + L_3 w_3 \\ L_1 \theta_1 + L_2 \theta_2 + L_3 \theta_3 \end{matrix} \right\} , \tag{6.124}$$

where

$$L_i = \frac{1}{2\Delta} \begin{vmatrix} x & t & 1 \\ x_j & t_j & 1 \\ x_k & t_k & 1 \end{vmatrix} , \tag{6.125}$$

and Δ is the surface area of a triangular element. The coefficients a_i can then be determined:

$$a_1 = \frac{1}{2\Delta} (t_{23} w_1 + t_{31} w_2 + t_{12} w_3) ,$$

$$a_2 = \frac{1}{2\Delta} (x_{32} w_1 + x_{13} w_2 + x_{21} w_3) , \tag{6.126}$$

$$a_3 = \frac{1}{2\Delta} (x_2 t_3 w_1 + x_3 t_1 w_2 + x_1 t_2 w_3) ,$$

where $x_{ij} = x_i - x_j$, $t_{ij} = t_i - t_j$. The coefficients b_i are computed in the same way. They contain the parameters of rotation θ_k instead of transverse displacements w_k. Total decoupling of the deflections and rotations results in the shape function matrix becoming diagonal:

$$\mathbf{N}_i = \begin{bmatrix} L_i & 0 \\ 0 & L_i \end{bmatrix} , \quad i = 1, 2, 3 . \tag{6.127}$$

The strains ε are described by the average share angle β and curvature κ

$$\varepsilon = \left\{ \begin{matrix} \beta \\ \kappa \end{matrix} \right\} = \left\{ \begin{matrix} \frac{\partial w}{\partial x} + \theta \\ \frac{\partial \theta}{\partial x} \end{matrix} \right\} . \tag{6.128}$$

The differential operator $\mathscr{D}$ contains two derivatives in terms of the variable x and has the form

$$\mathscr{D} = \begin{bmatrix} \frac{\partial}{\partial x} & 1 \\ 0 & \frac{\partial}{\partial x} \end{bmatrix} . \tag{6.129}$$

The constitutive relationship is described by the matrix of elasticity $\mathbf{E}$

$$\sigma = \left\{ \begin{matrix} Q \\ M \end{matrix} \right\} = \mathbf{E}\varepsilon = \begin{bmatrix} \frac{GA}{k} & 0 \\ 0 & EI \end{bmatrix} \varepsilon . \tag{6.130}$$

The next step is to determine the products, using the general formulas (6.15), (6.16), (6.19), and (6.20), and then integrate them in the area of the triangle. If we take the origin at the centre of gravity of the triangle, we can use the known rules

$$\int_\Delta dxdt = \Delta, \quad \int_\Delta xdxdt = 0, \quad \int_\Delta x^2 dxdt = \frac{\Delta}{12}\Sigma x_i^2, \quad \int_\Delta xt \, dxdt = \frac{\Delta}{12}\Sigma x_i t_i \,. \quad (6.131)$$

The resulting space–time stiffness matrix consists of 36 elements, in 2×2 frames, in each of the nodes. One of these frames $\mathbf{K}_{ij}^*$ is given below

$$\mathbf{K}_{ij}^* = \begin{bmatrix} \frac{GA}{4k\Delta}t_{kl}t_{mn}- & & \frac{GA}{4k\Delta}t_{kl}(x_mt_n - x_nt_m)+ \\ -\frac{\rho A}{4\Delta}x_{kl}x_{mn}+ & \vdots & +\frac{\eta_z}{4\Delta}t_{kl}x_{mn} \\ +\frac{\eta_z}{4\Delta}x_{mn}(x_kt_l - x_jt_k) & & \\ \cdots\cdots\cdots\cdots\cdots\cdots\cdots & & \cdots\cdots\cdots\cdots\cdots\cdots\cdots\cdots\cdots\cdots\cdots\cdots\cdots\cdots\cdots \\ & & \frac{EI}{4\Delta}t_{kl}t_{mn} - \frac{\rho I}{4\Delta}x_{kl}x_{mn}+ \\ & & +\frac{\eta_w+\eta_z}{4\Delta}(x_kt_l - x_lt_k)x_{mn}+ \\ \frac{GA}{4k\Delta}t_{mn}(x_kt_l - x_lt_k) & \vdots & +\frac{GA}{4k\Delta}\left[t_{kl}t_{mn}\frac{\Sigma x^2}{12} + x_{kl}x_{nm}\frac{\Sigma t^2}{12}+\right. \\ & & \left.+(t_{kl}x_{nm} + x_{lk}t_{mn})\frac{\Sigma xt}{12}\right]+ \\ & & \frac{GA}{4k\Delta}(x_kt_l - x_lt_k)(x_mt_n - x_nt_m) \end{bmatrix} . \quad (6.132)$$

Here we have used the following notation: $x_{ij} = x_i - x_j$, $t_{ij} = t_i - t_j$, $\Sigma x^2 = x_1^2 + x_2^2 + x_3^2$, $\Sigma t^2 = t_1^2 + t_2^2 + t_3^2$, $\Sigma xt = x_1t_1 + x_2t_2 + x_3t_3$.

Figure 6.31 shows the amplitude of the displacements of the free end of a cantilever loaded with a concentrated force with a Heaviside distribution, in relation to the value determined analytically. With the increase in the length of the elements b compared to the height H of the cross section, the accuracy decreases. With the length of the element equal to the height of the element's cross-section, the amplitude error reaches 24%.

6.7.3 Tetrahedral Space–Time Element of a Plate

We assume linear interpolation functions to describe the distribution of the generalized displacements in the space–time element domain. The vertical displacement w and the rotations in both x and y directions, i.e., θ_x and θ_y, will be expressed in terms of nodal parameters. The following polynomials of the first order are used
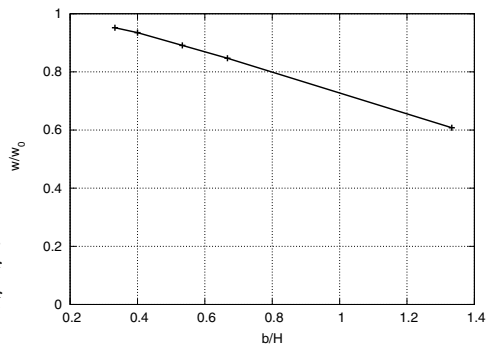
Fig. 6.31 The accuracy of the calculated displacements of the free end of the beam depending on the length of the spatial elements.

$$\begin{Bmatrix} w \\ \theta_x \\ \theta_y \end{Bmatrix} = \begin{Bmatrix} a_1x + b_1y + c_1t + d_1 \\ a_2x + b_2y + c_2t + d_2 \\ a_3x + b_3y + c_3t + d_3 \\ a_4x + b_4y + c_4t + d_4 \end{Bmatrix}. \tag{6.133}$$

The constants a_i, b_i, c_i, and d_i, $i = 1,2,3$ are determined from the relationships

$$\begin{Bmatrix} a_1 \\ b_1 \\ c_1 \\ d_1 \end{Bmatrix} = \mathbf{P}^{-1} \begin{Bmatrix} w_1 \\ w_2 \\ w_3 \\ w_4 \end{Bmatrix}, \quad \begin{Bmatrix} a_2 \\ b_2 \\ c_2 \\ d_2 \end{Bmatrix} = \mathbf{P}^{-1} \begin{Bmatrix} \theta_{x1} \\ \theta_{x2} \\ \theta_{x3} \\ \theta_{x4} \end{Bmatrix}, \quad \begin{Bmatrix} a_3 \\ b_3 \\ c_3 \\ d_3 \end{Bmatrix} = \mathbf{P}^{-1} \begin{Bmatrix} \theta_{y1} \\ \theta_{y2} \\ \theta_{y3} \\ \theta_{y4} \end{Bmatrix}, \tag{6.134}$$

where w_i, θ_{xi}, θ_{yi} are nodal displacements at node i. The matrix $\mathbf{P}$ then has the form

$$\mathbf{P} = \begin{bmatrix} x_1 & y_1 & t_1 & 1 \\ x_2 & y_2 & t_2 & 1 \\ x_3 & y_3 & t_3 & 1 \\ x_4 & y_4 & t_4 & 1 \end{bmatrix}. \tag{6.135}$$

If we denote by $\mathbf{r}_i$, $i = 1,\ldots,4$, the columns of the matrix $\mathbf{P}^{-1}$ and by $\mathbf{g}$ the vector of monomials

$$\mathbf{g} = [x,y,t,1], \tag{6.136}$$

then the shape functions of the tetrahedron are

$$\mathbf{N} = [\mathbf{N}_1, \mathbf{N}_2, \mathbf{N}_3, \mathbf{N}_4], \quad \mathbf{N}_i = \mathbf{g}\,\mathbf{r}_i, \quad i = 1,\ldots,4. \tag{6.137}$$

We define the strain vector ε by

$$\varepsilon = \left\{ \begin{array}{c} \kappa_x \\ \kappa_y \\ \kappa_{xy} \\ \beta_x \\ \beta_y \end{array} \right\} = \begin{bmatrix} 0 & \frac{\partial}{\partial x} & 0 \\ 0 & 0 & \frac{\partial}{\partial x} \\ 0 & \frac{\partial}{\partial y} & \frac{\partial}{\partial x} \\ \frac{\partial}{\partial x} & 1 & 0 \\ \frac{\partial}{\partial y} & 0 & 1 \end{bmatrix} \left\{ \begin{array}{c} w \\ \theta_x \\ \theta_y \end{array} \right\} = \mathscr{D}\,\mathbf{w} \; . \tag{6.138}$$

Here, $\mathbf{w}$ is the vector of displacements. The stress vector σ contains the bending moments m_x, m_y, and m_{xy} and shear forces q_x and q_y per unit length:

$$\sigma = \left\{ \begin{array}{c} m_x \\ m_y \\ m_{xy} \\ q_x \\ q_y \end{array} \right\} \; . \tag{6.139}$$

The elasticity matrix,

$$\mathbf{E} = \begin{bmatrix} D & \nu D & 0 & 0 & 0 \\ & D & 0 & 0 & 0 \\ & & \frac{1-\nu}{2}D & 0 & 0 \\ & & & H & 0 \\ & & & & H \end{bmatrix} \; , \quad D = \frac{t^3}{12}\frac{E}{1-\nu^2} \; , \quad H = \frac{5}{6}Gt \; , \tag{6.140}$$

where E is the Young modulus, ν is the Poisson coefficient, G is the shear modulus, and t is the thickness of the plate, allows us to write the stress–strain relation:

$$\sigma = \mathbf{E}\varepsilon \; . \tag{6.141}$$

The integration over the space–time tetrahedron is simplified if the origin of the coordinate system is placed at the centre of gravity of the element. We denote the entries of the matrix $\mathbf{P}^{-1}$ (6.135) by p_{ij}. Moreover, ρ is the mass density, η_w is the internal damping coefficient of the Kelvin–Voight model, η_z is the external damping coefficient, and V is the volume of the tetrahedral space–time element. Then the space–time stiffness matrix entries derived in terms of the displacements are as follows

$$K_{ij11} = HV(p_{1i}p_{1j} + p_{2i}p_{2j}) - \rho h p_{3i}p_{3j} ,$$

$$K_{ij12} = HV p_{1i}p_{4j} + \eta_w V p_{1i}p_{3j} ,$$

$$K_{ij13} = HV p_{2i}p_{4j} + \eta_w V p_{2i}p_{3j} ,$$

$$K_{ij21} = HV p_{4i}p_{1j} ,$$

$$K_{ij22} = DV p_{1i}p_{1j} + \frac{1-nu}{2} DV p_{2i}p_{2j} + \frac{HV}{20} p_{1i}p_{1j} \sum x_k^2 + \frac{HV}{20} p_{2i}p_{2j} \sum y_k^2 +$$

$$+ \frac{HV}{20} p_{3i}p_{3j} \sum t_k^2 + \frac{HV}{20} (p_{1i}p_{2j} + p_{2i}p_{1j}) \sum x_k y_k +$$

$$+ \frac{HV}{20} (p_{2i}p_{3j} + p_{3i}p_{2j}) \sum y_k t_k + \frac{HV}{20} (p_{1i}p_{3j} + p_{3i}p_{1j}) \sum x_k t_k +$$

$$+ HV p_{4i}p_{4j} - p_{3i}p_{3j} \frac{\rho h^3}{12} V + (\eta_w + \eta_z) V p_{4i}p_{3j} ,$$

$$K_{ij23} = vDV p_{1i}p_{2j} + \frac{1-nu}{2} DV p_{2i}p_{1j} ,$$

$$K_{ij31} = HV p_{4i}p_{2j} ,$$

$$K_{ij32} = vDV p_{2i}p_{1j} + \frac{1-nu}{D} V 2 p_{1i}p_{2j} ,$$

$$K_{ij33} = DV p_{2i}p_{1j} + \frac{1-nu}{2} DV p_{1i}p_{1j} + \frac{HV}{20} p_{1i}p_{1j} \sum x_k^2 + \frac{HV}{20} p_{2i}p_{2j} \sum y_k^2 +$$

$$+ \frac{HV}{20} p_{3i}p_{3j} \sum t_k^2 + \frac{HV}{20} (p_{1i}p_{2j} + p_{2i}p_{1j}) \sum x_k y_k +$$

$$+ \frac{HV}{20} (p_{2i}p_{3j} + p_{3i}p_{2j}) \sum y_k t_k + \frac{HV}{20} (p_{1i}p_{3j} + p_{3i}p_{1j}) \sum x_k t_k +$$

$$+ HV p_{4i}p_{4j} - p_{3i}p_{3j} \frac{\rho h^3}{12} V + (\eta_w + \eta_z) V p_{4i}p_{3j} .$$

$$(6.142)$$

The test problem depicted in Figure 6.32 results in amplitudes which are there compared with other results collected in Table 6.5.

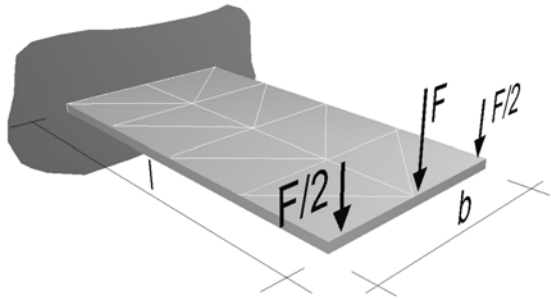**Fig. 6.32** Test problem — a cantilever plate.

Table 6.5 Summary results of calculations of test analysis of a disc.

mesh	No. of nodes	deflection w	period T	$\frac{Dw}{QL^2}$	$\frac{\omega}{\sqrt{D/\rho t L^4}}$
2×1	6	318.	109.	0.564	4.84
4×2	15	537.	133.	0.953	3.97
8×4	45	720.	157.	1.277	3.37
Other results for comparison*:					
— Ritz method					3.47
— experimental					3.42
— Plunkett'e experiments					3.50
— finite elements (modal analysis)					
— 2×1 (4 triangular elements)					3.39
— 4×2 (16 triangular elements)					3.44

*O.C. Zienkiewicz, *The Finite Element Method in Engineering Science*,
2nd edition, McGraw-Hill, 1971

6.8 Triangular Elements Expressed in Velocities

The final system of equations obtained using the velocity formulation has the same
features as when the displacement formulation is used. We will try to construct a
model of a triangular element of an axially vibrating rod and investigate its proper-
ties. The accuracy of the calculated amplitudes, the periods of the free vibrations,
and the stability of solutions obtained by using these elements will be important
when we evaluate the velocity simplex elements.

The virtual power equation (6.61) is used to build a recursive matrix equation.
Below we will use triangular elements. In the beginning, let us take two comple-
mentary triangles, shown in Figure 6.33. The principle of virtual work (6.62) allows
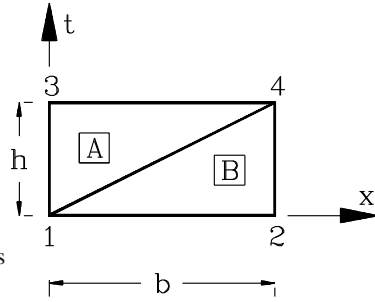us to write

Fig. 6.33 Triangular system of elements described with velocities.

$$\int_{\Omega} (\mathbf{N}^*)^T \rho A \frac{\partial v}{\partial t} d\Omega + \int_{\Omega} \frac{\partial (\mathbf{N}^*)^T}{\partial x} EA \frac{\partial}{\partial x} \left[\int_{t_0}^{t} v dt \right] d\Omega = 0 . \tag{6.143}$$

Here, $\mathbf{N}^*$ is the matrix of virtual shape functions, v is the velocity at the point (x,t), Ω is the domain of the triangle A or B, and E, ρ, A are the Young modulus, mass density and cross sectional area, respectively. In the element A the real velocity is described by

$$v_A(x,y) = \mathbf{N}_A(x,t) \mathbf{v} = \left[1 - \frac{t}{h}, \frac{x}{b}, -\frac{x}{b} + \frac{t}{h} \right] \mathbf{v} , \tag{6.144}$$

and the virtual functions in nodes 3 and 4 have the form

$$\mathbf{N}_A^*(x,t) = \left[-\frac{x}{b} + \frac{t}{h}, \frac{x}{b} \right] . \tag{6.145}$$

Inertia matrix is then determined from the relation

$$\mathbf{M}_A = \int_0^b \int_{\frac{hx}{b}}^{h} (\mathbf{N}_A)^T \rho A \frac{\partial}{\partial t} \mathbf{N}_A \, dt \, dx = \rho A \frac{b}{6} \begin{bmatrix} -1 & 0 & 1 \\ -1 & 0 & 1 \end{bmatrix} . \tag{6.146}$$

The real shape functions and the virtual function of the node 4 in the element B have the following forms

$$\mathbf{N}_B = \left[1 - \frac{x}{b}, \frac{x}{b} - \frac{t}{h}, \frac{t}{h} \right], \quad \mathbf{N}_B^* = \frac{t}{h} . \tag{6.147}$$

The mass matrix is thus

$$\mathbf{M}_B = \rho A \frac{b}{6} [0, -1, 1] . \tag{6.148}$$

The stiffness matrices described in the second part of the equation (6.143) have the following form

$$\mathbf{K}_A = \int_0^b \int_{\frac{hx}{b}}^{h} \frac{\partial (\mathbf{N}_A^*)^T}{\partial x} EA \frac{\partial}{\partial x} \left[\int_0^t \mathbf{N}_A dt \right] dt \, dx = EA \frac{h^2}{3b} \begin{bmatrix} 0 & -1 & 1 \\ 0 & 1 & -1 \end{bmatrix} ,$$

$$\mathbf{K}_B = \mathbf{0} . \tag{6.149}$$

The initial force vector in the element is

$$\mathbf{s} = EA \int_0^b \int_{\frac{hx}{b}}^h \frac{\partial (\mathbf{N}_A^*)^T}{\partial x} \frac{\partial w(t_0)}{\partial x} \, dt \, dx = EA\varepsilon_0 \frac{h}{2} \begin{bmatrix} -1 \\ 1 \end{bmatrix} . \tag{6.150}$$

We can use the transformed form of (6.143):

$$\frac{1}{4\Delta}(x_m t_n - x_n t_m) \sum_i x_{kj} v_i + \frac{t_{mn}}{2} \varepsilon_0 - \frac{1}{4\Delta} t_{mn} t_0 \sum_i x_{jk} v_i = 0 , \tag{6.151}$$

where Δ is the surface area of the triangle, $t_{mn} = t_m - t_n$, $x_{kj} = x_k - x_j$, and t_0 is the time location of the node with the lowest coordinate t_i in the coordinate system with origin at the centre of gravity of the triangle.

The global arrays of the system allow us to write a recursive equation:

$$\left(\frac{1}{6} \begin{bmatrix} -1 & 0 \\ -1 & -1 \end{bmatrix} \begin{vmatrix} 1 & 0 \\ 1 & 1 \end{vmatrix} + \frac{c^2 h^2}{3b^2} \begin{bmatrix} 0 & 0 \\ 0 & 0 \end{bmatrix} \begin{vmatrix} 1 & -1 \\ -1 & 1 \end{vmatrix} \right) \mathbf{v} + \frac{h}{2b} c^2 \varepsilon_0 \begin{bmatrix} -1 \\ 1 \end{bmatrix} = \mathbf{0} . \tag{6.152}$$

If we fix the right degree of freedom, we obtain an oscillating system with one degree of freedom, described by the system of equations

$$\begin{cases} v_{i+1} = \frac{(1-2\kappa^2)v_i + 3\varepsilon_i}{1+\kappa^2} , & \kappa = \frac{ch}{b} , \\ \varepsilon_{i+1} = \varepsilon_i - \left(\frac{2}{3}v_i + \frac{1}{3}v_{i+1} \right) \frac{h}{b} . \end{cases} \tag{6.153}$$

The period of oscillations of the oscillator modelled by the system (6.153) (with unit values for E, S, ρ, b) is 3.628, whereas the exact value is $2\pi/\sqrt{3} \approx 3.6276$.

The derived matrices were tested by examples. The task was an axially vibrating rod, divided into 20 spatial elements. The meshes of type a and b are shown in Figure 6.34. In order to compare the results, the task was solved with the use of a mesh of rectangular elements, with parameter $\alpha = 1/2$. In all cases, the time step was $h = 0.01$. The displacements of the free end of the bar in time, as the system response, are shown in Figure 6.34. Comparing the graphs, one can see the correct behaviour of the given system. The amplitudes of the parasitic frequencies are small. The difference illustrated in Figures 6.34a and 6.34b results from the manner in which the initial conditions were introduced. In the case of a, the initial speed $v_0 = 1$ was applied to the extreme node, which belongs to only one triangle. In case b, the extreme node at $t = 0$ joins two triangular elements. Finally, in this way of loading, the grid b better models the propagation of pulses. The stiffness matrices in the case of a grid consisting of two triangles (e.g. Figure 6.33) can also be derived in a simpler manner. We must calculate the work of the internal forces on the virtual displacements in the domain $0 \le x \le b$, $0 \le t \le h$. For example, if we take the system shown in Figure 6.34a, the increment of deformations in the interval $[0, h]$, calculated at $x = b/3$, and thus at the centre of gravity of the left triangle, is

$$\Delta\varepsilon = \frac{2}{3}h\frac{v_2 - v_1}{b} + \frac{1}{3}h\frac{v_4 - v_3}{b} . \tag{6.154}$$
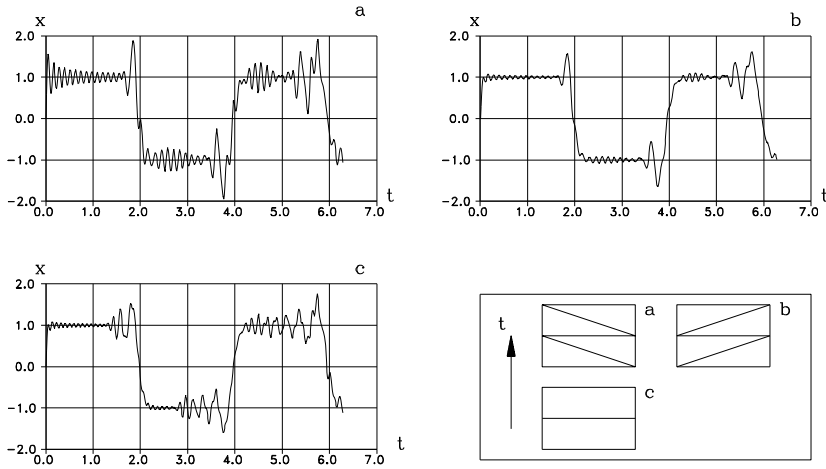
Fig. 6.34 Displacements in time of the free end of the rod with triangular and rectangular meshes (20 spatial elements).
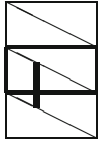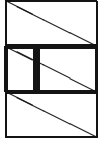
Finally, we get the matrix
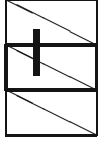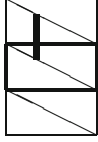
$$\frac{EAh^2}{6b} \left[\begin{array}{cc|cc} 2 & -2 & 1 & -1 \\ -2 & 2 & -1 & 1 \end{array} \right] . \tag{6.155}$$

The displacements at the end of the interval $[0,h]$ are determined by the formula $x_1 = x_0 + hv_0$. The system response does not depend on which time we calculate the strain increment or on how situated the time interval of length h along which the integration is carried out. Sample diagrams with the corresponding stiffness matrices are given in Table 6.6. The first set of options there is conditionally stable. Others are unconditionally stable due to the time step. Assuming the inertia matrix given in (6.146) and (6.148), summed in (6.152), and the stiffness matrix of the system according to the first system in Table 6.6, we obtain triangular matrices of coefficients (right submatrix, associated with $\mathbf{v}_{i+1}$).

Triangular elements are ideal for refining and coarsening the grid over time. We can also modify the mesh in selected spatial areas and decrease the time step (Figure 6.35). A subintegration in time carried out in selected areas enables us, for example, to easilydescribe the contact. In Figure 6.35b, two joints are introduced: t_c is the entry of the point into contact and t_f is the end of the contact interval. In practice, the whole space–time layer, i.e., all the nodes placed at t_{i+1} and the supplementary nodes (sub–division), are treated in the same stage of calculations, in one matrix equation.

Table 6.6 Stiffness matrices in the different schemes.

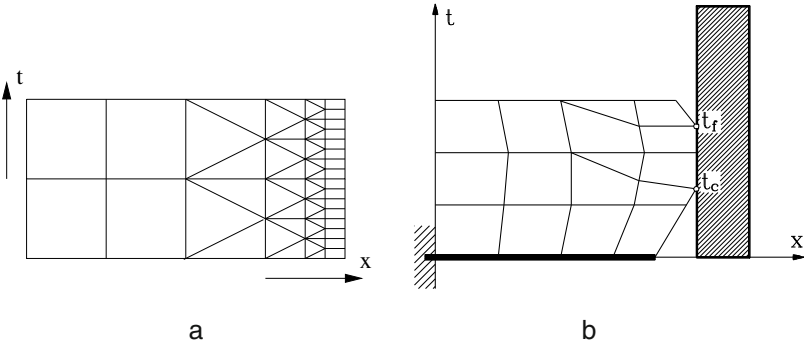| scheme	stiffness matrix
	$\dfrac{EAh^2}{6b} \begin{bmatrix} 3 & -3 & 0 & 0 \\ -3 & 3 & 0 & 0 \end{bmatrix}$
	$\dfrac{EAh^2}{6b} \begin{bmatrix} 2 & -2 & 1 & -1 \\ -2 & 2 & -1 & 1 \end{bmatrix}$
	$\dfrac{EAh^2}{6b} \begin{bmatrix} 1 & -1 & 2 & -2 \\ -1 & 1 & -2 & 2 \end{bmatrix}$
	$\dfrac{EAh^2}{6b} \begin{bmatrix} 0 & 0 & 3 & -3 \\ 0 & 0 & -3 & 3 \end{bmatrix}$

Fig. 6.35 Examples of grid refinement in time-space using triangular elements: a) general idea, b) scheme used for contact problems.